JOURNAL OF GEOPHYSICAL RESEARCH, VOL. 107, NO. D19, 4391, doi:10.1029/2001JD001191, 2002

Moisture budget of the Arctic atmosphere from TOVS satellite data

David G. Groves
RAND Corporation, Santa Monica, California, USA

Jennifer A. Francis
Institute of Marine and Coastal Sciences, Rutgers University, New Brunswick, New Jersey, USA

Received 8 August 2001; revised 23 January 2002; accepted 23 January 2002; published 9 October 2002.

[1] The Arctic atmospheric moisture budget is an important component of the Arctic climate system, and moisture transport is a major mechanism by which both local and hemispheric atmospheric processes affect the Arctic Ocean. The lack of humidity data over the Arctic Ocean severely hampers present understanding of climatological and time-varying features of the Arctic moisture budget. We combine daily satellite precipitable water retrievals from the NASA/NOAA TIROS Operational Vertical Sounder (TOVS) Polar Pathfinder data set with wind fields from the NCEP-NCAR Reanalysis to create a new high-resolution data set of the Arctic atmospheric moisture budget from October 1979 to December 1998. Products are at a horizontal resolution of $(100\ \text{km})^2$ and include daily fields of precipitable water and precipitable water flux profiles at 16 vertical levels and net precipitation (i.e., precipitation minus evaporation, *P-E*). We show that these retrievals compare well with rawinsonde-derived moisture transport and reanalysis products, yet capture spatial and temporal variability that other data sets cannot owing to the sparse coverage of the conventional observation network in the Arctic Ocean. Our method yields an average annual net precipitation of 15.1 cm yr^{-1} over the polar cap (poleward of 70°N) and 12.9 cm yr^{-1} over the Arctic Basin. Poleward moisture transport into the Arctic is greatest from June to August and smallest in December. Over regions of known storm tracks, especially in the North Atlantic sector, we find that transient circulation features account for 32% of the net precipitation in the Greenland-Iceland-Norwegian Seas, 90% in the Nansen Basin, and 74% in the Arctic basin as a whole. *INDEX TERMS:* 3349 Meteorology and Atmospheric Dynamics: Polar meteorology; 3354 Meteorology and Atmospheric Dynamics: Precipitation (1854); 1823 Hydrology: Frozen ground; 3360 Meteorology and Atmospheric Dynamics: Remote sensing; 1655 Global Change: Water cycles (1836); *KEYWORDS:* Arctic, precipitation, hydrology, satellite, climate, polar

Citation: Groves, D. G., and J. A. Francis, Moisture budget of the Arctic atmosphere from TOVS satellite data, *J. Geophys. Res.*, *107*(D19), 4391, doi:10.1029/2001JD001191, 2002.

1. Introduction

[2] The atmospheric moisture budget is a critical component of the Arctic climate system. Winds transport moisture from low to high latitudes, where some of the moisture condenses to form clouds and precipitates as snow and rain. A thin snowfall increases the albedo of sea ice and greatly influences the surface energy balance. Arctic cloud cover affects surface radiation fluxes and radiative heating of the atmosphere. These, in turn, affect surface temperature, ice growth and melt, and upper ocean salinity. Finally, precipitation minus surface evaporation (net precipitation; *P-E*) is a direct flux of freshwater to the surface of the ice pack and the ocean. The freshwater budget of the ocean surface is important to the Arctic and global climate for several reasons. First, freshwater maintains the upper ocean's strong stratification and therefore influences sea ice growth, thickness, and extent. Upper ocean salinity also may influence the location and strength of Arctic deep water formation, which partially drives the global ocean thermohaline circulation [*Broecker*, 1994].

[3] Recently many disturbing changes have been observed in the Arctic. Among these are a decreasing average sea ice extents [*Gloersen et al.*, 1992; *Johannessen et al.*, 1999; *Maslanik et al.*, 1996; *Maslanik et al.*, 1999; *Cavalieri et al.*, 1997], a 40% reduction in sea ice thickness [*Rothrock et al.*, 1999], freshening and warming of the upper ocean [*Morison et al.*, 1998; *Steele and Boyd*, 1998], rising surface temperatures [*Martin and Munoz*, 1997; *Rigor et al.*, 2000], decreasing sea level pressure [*Walsh et al.*, 1996; *Thompson and Wallace*, 1998], and increasing cyclone activity [*Serreze et al.*, 1997; *Key and Chan*, 1999]. Many of these changes are summarized by *Serreze*

0148-0227/02/2001JD001191$09.00

et al. [2000]. These alarming observations have heightened interest in assessing the role of hydrologic processes in these changes.

[4] The atmospheric moisture budget can be expressed generically as

$$P - E = \frac{(-\nabla \cdot \vec{F})}{\rho_w} - \frac{\partial Q}{\partial t} \quad \text{and} \tag{1}$$

$$\vec{F} = \frac{1}{g} \int (q\vec{V}) dp \tag{2}$$

where *P-E* is precipitation minus evaporation (net precipitation), $\vec{F}$ is the vertically integrated precipitable water mass flux, ρ_w is the density of liquid water (1000 kg m^{-3}), $(-\nabla \cdot \vec{F})/\rho_w$ is the vertically integrated precipitable water (*PW*) flux convergence, Q is the vertically integrated precipitable water (by volume), $\partial Q/\partial t$ is its tendency, q is the specific humidity (kg kg^{-1}), $\vec{V}$ is the horizontal wind vector (m s^{-1}), g is the gravitation constant (m s^{-2}), and P is pressure (Pa) integrated from the surface to the top of the atmosphere. Dimensions for each of the three terms in equation (1) are water volume per unit area per time, which is usually expressed as equivalent water depth per unit time. The actual equations used in our analysis are

$$(P - E)_{i,j} = \left(\sum_{k=0}^{top} \left(-(\nabla \cdot Q_k \vec{V}_k) - \frac{\partial Q_k}{\partial t} \right) \right)_{i,j} \quad \text{and} \tag{3}$$

$$\vec{F}_{i,j} = \left(\sum_{k=0}^{top} (Q_k \vec{V}_k) \right)_{i,j}, \tag{4}$$

where Q_k is the modified TOVS-retrieved *PW*, $\vec{V}_k$ is the horizontal wind vector from the NCEP-NCAR reanalysis, i and j specify the horizontal grid point, and k designates the sigma level defined in the reanalysis. In this study we use surface pressure fields from the NCEP-NCAR reanalysis data set [*Kalnay et al.*, 1996] to establish the lower boundary of the sigma vertical coordinate. The vertically integrated flux $\vec{F}$ at each grid point is calculated using equation (4), which is a summation of the vapor fluxes at each level. The horizontal *PW* flux convergence minus the change in *PW* storage over a time step equals the vertical *PW* transport into or out of the layer.

[5] Estimates of total liquid water and ice content of Arctic clouds range from 0.01 g m^{-3} to 0.60 g m^{-3} [*Radionov et al.*, 1997], which equates to between 10^{-3} and 6×10^{-2} mm equivalent liquid water per km of cloud thickness. Cloud thickness rarely exceeds 1 km for the predominantly low-level Arctic clouds. Therefore, the total liquid water and ice amount will always be less than 1% of the water vapor and can therefore be ignored in moisture flux and flux convergence calculations. Using equations 1 and 2, we compute the moisture exchange between the atmosphere and the surface by knowing only the wind fields and precipitable water profiles. This ''aerological'' approach to estimating net precipitation is widely used.

[6] Notation for the terms in equations 1 and 2 varies throughout the literature. Our notation attempts to conform to standard atmospheric science conventions. It is customary to refer to net precipitation, computed using the right-hand-side (rhs) of equation 1, as *P-E*. To eliminate any confusion between this computed *P-E* and the actual difference between precipitation and evaporation estimates or measurements, we refer to the solution of the rhs of equation 1 as $(P\text{-}E)_{calc}$. On annual timescales, precipitable water tendency is negligible [*Pexioto and Oort*, 1992] and $P - E = (-\nabla \cdot \vec{F})/\rho_w$. For time periods shorter than a year, precipitable water tendency is not negligible, as we show in section 5.2.

[7] In this study, we compute the moisture budget for a 19-year period (1980 to 1998) by combining TOVS satellite retrievals of precipitable water on the daily, $(100\ km)^2$ EASE (Equal-Area SSM/I Earth) grid with wind and surface pressure fields from the NCEP-NCAR Reanalysis data set [*Kalnay et al.*, 1996]. This approach is desirable first because the satellite moisture retrievals are dense in space and time and are not subjected to assimilation or interpolation schemes employed to create reanalysis and rawinsonde data sets. Note that the NCEP-NCAR reanalysis does not assimilate satellite-derived moisture information in the Arctic. Second, our derived net precipitation does not depend upon modeling poorly understood and observed Arctic precipitation and evaporation processes, which cannot be said for reanalyses.

[8] In section 2 we summarize previous approaches to examining the Arctic atmospheric moisture budget. We utilize several different data sources and introduce new processing steps and methodologies to compute the moisture budget using satellite retrievals. In section 3, we discuss major data sources, validation, and processing steps used. In section 4 we describe the methodology used to create a high temporal and spatial resolution moisture budget from satellite precipitable water retrievals and reanalysis wind fields for the 19-year record of the TOVS instrument. Finally, in section 5 we describe the climatological characteristics of the annual-mean moisture budget and compare the annual totals and annual cycles with others.

[9] *Groves and Francis* [2002] compare winter and summer patterns in the moisture budget, describe decadal differences in the moisture budget, and explore the relationship between the Arctic Oscillation (the primary mode of circulation variability in the Northern Hemisphere) and the moisture budget.

2. Previous Research

[10] Characterizing the Arctic moisture budget, especially its spatial structure and temporal variability, is hindered by the sparseness of direct observations. Several methods have been used to estimate components of the moisture budget, including (1) creating surface flux climatologies from surface observations of *P* and *E*, (2) computing atmospheric moisture flux and flux convergence from rawinsonde measurements, and (3) examining forecast precipitation and evaporation as well as computed net precipitation, $(P\text{-}E)_{calc}$, from gridded reanalysis data sets.

2.1. Surface Estimates

[11] Climatological surface moisture fluxes (precipitation and evaporation) have been estimated using data from Russian meteorological stations drifting on the Arctic sea

ice. *Serreze and Hurst* [2000] created a monthly precipitation climatology over the Arctic by blending Russian ice station precipitation estimates with a modified version of the *Legates and Willmott* [1990] precipitation climatology. This is believed to be the most accurate climatology available at present.

[12] Determining evaporation rates over the entire Arctic is extremely difficult, as there are few direct measurements of evaporation. Climatological evaporation rates have been estimated using a standard bulk aerodynamic formula with measurements of the near-surface vertical gradient of specific humidity and wind speed from drifting ice stations [*Briazgin et al.*, 1996]. This approach is problematic, however, as these parameters are highly heterogeneous over sea ice. To estimate daily or monthly evaporation fields, high-resolution near-surface data are required, which at present do not exist.

2.2. Calculations With Rawinsondes

[13] Atmospheric moisture, moisture transport, and moisture flux convergence have been studied extensively using rawinsonde data. *Nakamura and Oort* [1988] and *Masuda* [1990] calculate the transport of moisture across an imaginary wall along the 70°N latitude circle, and separate the moisture flux into contributions by the mean meridional circulation, standing eddies, and transient eddies. We perform a similar analysis and compare our results with theirs in section 5.2. *Serreze et al.* [1994] utilize all available launches from 1974 to 1991 in the Arctic region to produce a water vapor climatology. *Walsh et al.* [1994] and *Serreze et al.* [1995b] compute climatological moisture fluxes and flux convergence using moisture and wind data from rawinsondes. *Serreze and Barry* [2000] summarize the current understanding of the moisture budget based on rawinsonde data, and we compare our results to theirs in sections 5.1 and 5.2. While these data successfully identify the climatological moisture pathways and basin-wide moisture convergence, their results have large uncertainties over the central Arctic Ocean where rawinsondes are sparse. Fields of moisture data are highly sensitive to the treatment of missing station data and interpolation between stations [*Serreze et al.*, 1995a; *Cullather et al.*, 2000], and soundings may have larger uncertainties in extreme cold [*Gaffen and Elliott*, 1993; *Serreze et al.*, 1995a].

2.3. Reanalysis Studies

[14] Moisture budget products from the NCEP-NCAR (National Center for Environmental Prediction-National Center for Atmospheric Research) Reanalysis and the ECMWF (European Centre for Medium-Range Weather Forecasts) Reanalysis (ERA) are attractive for Arctic studies, as they use ''frozen'' versions of the models and have relatively high spatial and temporal resolution, but they also have significant deficiencies, as described below.

2.3.1. Precipitable Water

[15] Comparisons of the reanalysis *PW* values to those from a variety of Arctic rawinsonde archives generally agree [*Bromwich et al.*, 2000]. They should be nearly equal, in fact, at the location and time of the rawinsonde measurements, as the reanalysis models assimilate these data.

[16] *Bromwich et al.* [2000] evaluate reanalysis fields of *PW* by comparing them with independent in situ measurements in regions where data are sparse. They find that the annual mean *PW* from the NCEP-NCAR reanalysis data is 0.9 mm less (or 16% lower) than the annual average *PW* measured by Russian drifting ice station 28, which was in operation from June, 1986 to December, 1988 in the central Arctic. The authors suggest that data from this station may not have been assimilated by the NCEP model, implying that the reanalysis *PW* fields may be significantly in error in regions that are not near assimilated data, which includes most of the Arctic Ocean. The comparison between the ERA and NP-28 *PW* is much better, either indicating that the ERA model assimilated the NP-28 data, or that the ERA moisture processes are more realistically simulated over the Arctic than those in the NCEP reanalysis model.

[17] To investigate this further, we examine the differences between the analysis field of *PW* and the 6-hour forecast field for the same time as the analysis (generated from the previous 6-hour analysis) from NCEP-NCAR for June, 1995. At the site of the NP-26 drifting station in the central Arctic, the monthly mean difference in *PW* between the analysis and the previous time step's forecast for that same time as the analysis is approximately 15% (based on 120 comparisons) (Figure 1). Elsewhere in the basin, where no assimilation sites exist, the difference is less than 2.5%. This suggests that where data are assimilated, the NCEP-NCAR model corrects the *PW* field, up to 15% in this example. The model does not, however, adjust the *PW* fields elsewhere. Assuming consistent model performance, semi-permanent errors must exist over data-sparse areas of the Arctic, and the *gradients* of precipitable water are highly erroneous over localized regions within the influence of assimilation sites. Moreover, operational moisture retrievals from TOVS are not assimilated into the NCEP reanalysis over the Arctic, according to observation counts available on the NCEP-NCAR Reanalysis website.

2.3.2. Precipitation, Evaporation, and *P-E*

[18] *Serreze and Hurst* [2000] evaluated *P-E* fields produced by NCEP-NCAR and ERA reanalysis projects by comparing them to a data set consisting of Russian ice station precipitation estimates blended with a modified version of the *Legates and Willmott* [1990] precipitation climatology. They found that while both reanalyses capture the general annual-mean spatial patterns and seasonal cycles, the reanalyses underestimate precipitation in the Atlantic side of the Arctic basin. ERA's simulations of precipitation and evaporation appear to be more realistic overall than those from NCEP-NCAR. The NCEP-NCAR estimates of *P-E* appear reasonable, but it is because large over-estimates of precipitation are compensated by excessive evaporation. Their fields also exhibit a lobed pattern, termed ''spectral snow'', which is caused by a poor approximation of vapor diffusion. They conclude that NCEP-NCAR's assimilation procedure may be rejecting valuable moisture data and that poor cloud parameterizations may be contributing to the problems in *P* and *E*.

[19] *Cullather et al.* [2000] examine both computed $(P\text{-}E)_{\mathrm{calc}}$ (rhs of equation 1) and forecast *P* minus forecast *E* from the reanalysis data sets. They find large differences between the moisture balance from these methods: the forecast *P-E* is 73% (38%) smaller than $(P\text{-}E)_{\mathrm{calc}}$ for NCEP-NCAR (ERA) products. They also compare the

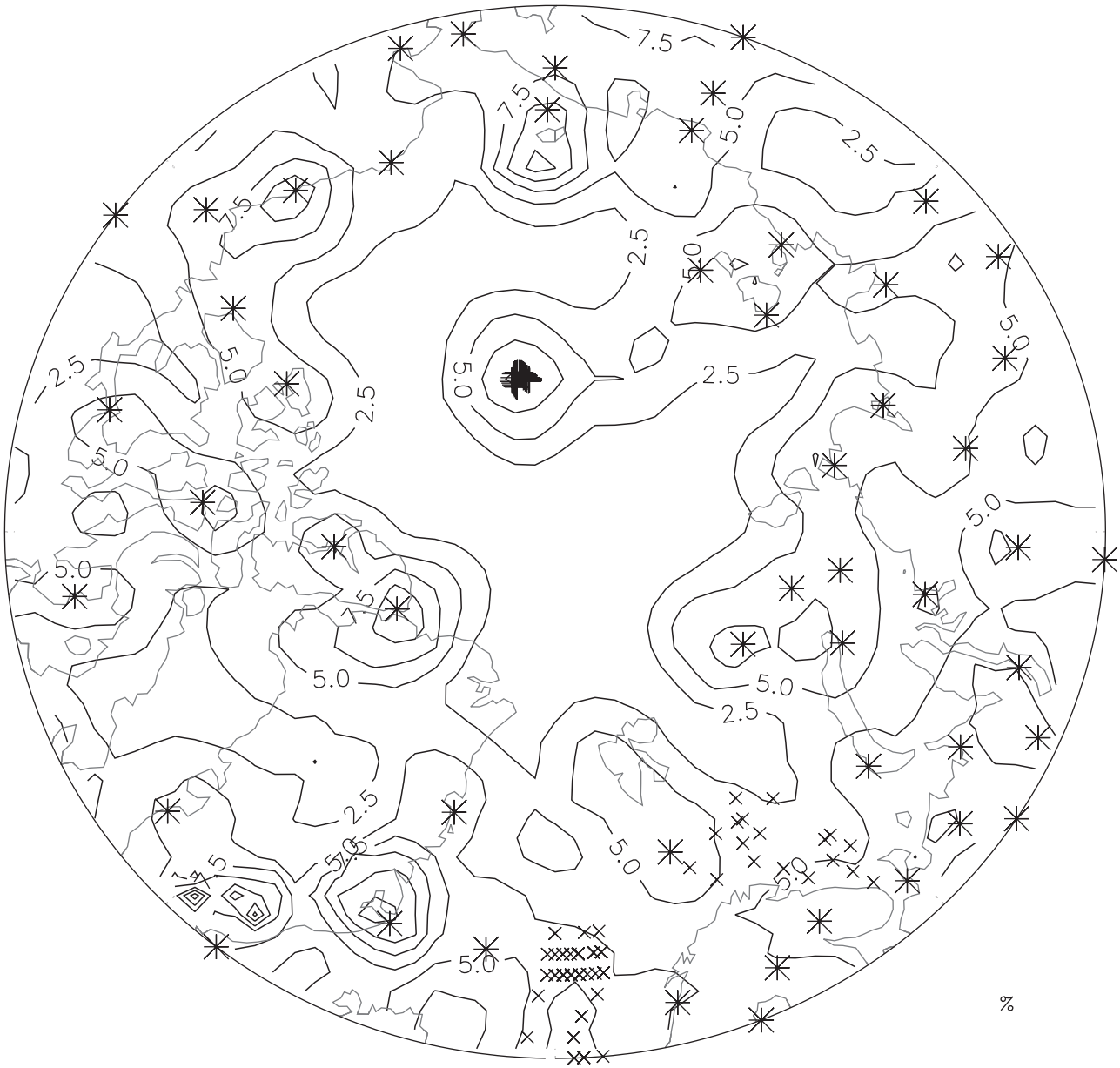

Figure 1. Composite map of error magnitude expressed as percent of 6-hourly forecast precipitable water for June, 1985. Plus symbols indicate the positions of Russian ice station NP-26, crosses indicate marine rawinsonde launch locations from the NCEP Marine rawinsonde archive, and the asterisks indicate the location of HARA land-based stations in operation during June, 1985. Contour interval is 2.5%. Error is defined as the forecast value minus the analysis value all over the analysis value times 100%.

reanalysis $(P\text{-}E)_{calc}$ fields with rawinsonde estimates. Although they show annual reanalysis estimates of moisture flux convergence between 70° and 90°N to be approximately 20% greater than estimates from rawinsonde data, they suggest that this may be due to deficiencies in the rawinsonde network. As discussed in section 2.3.1, however, significant errors do exist in the NCEP-NCAR *PW* fields, which contribute to documented errors in *P-E* derived from them.

[20] This discussion illustrates the need for improved fields of hydrologic parameters over the Arctic region. Successful validation of TOVS retrievals with rawinsonde data suggests that the recently available 19-year record of daily, $(100\ km)^2$ *PW* fields from TOVS represents a valuable source of information for calculating more accurate estimates of net precipitation over the Arctic Ocean.

3. Data Sources and Processing

[21] This study is the first to use satellite moisture retrievals to examine the Arctic atmospheric moisture budget. By combining satellite moisture retrievals with reanalysis wind fields, daily moisture transport and convergence are calculated throughout the Arctic, which cannot be done with

only rawinsonde data, while remaining independent of reanalysis moisture assimilation schemes. Several important steps are taken to blend the different data types in a coherent, optimal way.

[22] First, rawinsonde data from three archives are used, along with TOVS cloud fraction estimates, passive microwave sea ice concentration fields, and digital elevation data, to identify and correct biases in the TOVS Path-P precipitable water retrievals (section 3.2.2). Rawinsonde data allow the construction of climatological relative humidity profiles, which are combined with TOVS Path-P temperature retrievals to vertically distribute the TOVS precipitable water within each retrieval layer (section 4). Finally, daily NCEP-NCAR wind fields are used with the modified precipitable water retrievals in a moisture budget equation to calculate daily *PW* flux and flux convergence over the Arctic Ocean (section 4).

3.1. Rawinsonde Data

[23] Rawinsonde data from three major archives that cover the Arctic are used: (1) the Russian North Pole (NP) archive consisting of 19 drifting sea ice stations from the mid-1950s to 1990 [*National Snow and Ice Data Center* (*NSIDC*), 1997a; *Kahl et al.*, 1999], (2) the NCEP Arctic Marine Rawinsonde Archive that contains 17,659 commercial and military ship rawinsonde launches north of 65°N from 1976 to 1996 [*NSIDC*, 1997b], and (3) the Historical Arctic Rawinsonde Archive (HARA) that contains millions of soundings from Arctic land stations during the late 1950s to 1996 [*Serreze et al.*, 1992]. Only data from 1979–1998 are used, corresponding to the TOVS data availability. Monthly climatologies of precipitable water have also been created from these data by *Serreze et al.* [1994]. We use the monthly climatological fields of total precipitable water to compare spatial patterns of precipitable water to those from TOVS. All four data sets were obtained from the NASA/EOS (Earth Observing System) Distributed Active Archive Center (DAAC) at the National Snow and Ice Data Center, University of Colorado, Boulder, CO.

[24] The NP data are used to create monthly mean climatological relative humidity (*RH*) profiles representative of ice-covered regions as well as marine rawinsondes to create analogous profiles for open-ocean regions within the Arctic basin and North Atlantic. Monthly climatological *RH* profiles are also computed for each permanent land-based station contained in the HARA archive to capture the large spatial variability over land. We then interpolate the HARA *RH* profiles from the land-based rawinsonde network to the over-land portion of the three-dimensional grid used in this study. Finally, all monthly *RH* climatologies are linearly interpolated in time to create daily profiles. Procedures for screening erroneous rawinsonde launches and creating *RH* profiles are based on procedures developed by *Serreze et al.* [1994] and are described in more detail in *Groves* [2001]. Resulting profiles are used in conjunction with the TOVS retrievals of precipitable water and temperature, as described in section 4.

3.2. NASA/NOAA TOVS Polar Pathfinder (Path-P) Data Set

[25] The TIROS-N operational vertical sounder (TOVS) has flown aboard NOAA polar orbiting satellites from 1979 to the present. The Improved Initialization Inversion (so-called "3I") method, developed at the Laboratoire de Météorologie Dynamique du CNRS, in Palaiseau, France [*Chédin et al.*, 1985; *Scott et al.*, 1999], along with polar improvements to the retrieval scheme by *Francis* [1994], have been used to create a high-quality Arctic data set called the NASA/NOAA TOVS Polar Pathfinder (Path-P) data set. Products include daily averaged retrievals of numerous atmospheric and surface variables over the Arctic, including temperature at 10 levels (50, 70, 100, 300, 400, 500, 600, 700, 850, and 900 hPa), layer-averaged precipitable water (bounded by 300, 400, 500, 700, 850 hPa, and the surface), surface skin temperature, cloud fraction, and others. The products are gridded at a $(100\ km)^2$ resolution for the years 1979–98 and are available from the National Snow and Ice Data Center (http://nsidc.org).

[26] The NOAA polar-orbiting satellites provide excellent coverage of the Arctic; approximately 14 views of a particular location per day per satellite. Data for some days are missing because of satellite error or data corruption, although only 5 months out of a total of 231 used in this study are missing more than 4 days of data. This excellent temporal coverage allows us to create robust monthly climatologies.

3.2.1. Validation

[27] Validation studies show that the TOVS retrievals of temperature and precipitable water agree well with in situ measurements from rawinsondes at North Pole (NP) Russian drifting sea ice stations [*Francis and Schweiger*, 2000] and with measurements from the Surface Heat Budget of the Ocean (SHEBA) rawinsonde archive [*Schweiger et al.*, 2002]. The SHEBA field program was located in the Beaufort Sea and drifted from ~75°N, 145°W, in October 1997, to ~80°N, 165°W, in October 1998. The NP comparison shows the root mean squared (RMS) error for precipitable water to range between 1 mm in winter and 2 mm in summer (~20%). For the SHEBA comparison, the RMS error is ~2.2 mm and the two records correlate at $r = 0.88$. Although difficult to quantify, some of the uncertainty results from the comparison of a spatially averaged quantity (TOVS) with daily averaged, point measurements (rawinsondes), and some is likely due to error in the rawinsonde data themselves.

[28] Because TOVS-derived precipitable water is the fundamental parameter used in this study, we compare a larger subset of rawinsonde launches from NP drifting ice stations with the nearest precipitable water retrieval. Our findings show a similar high correlation between rawinsonde-measured *PW* and TOVS-retrieved *PW* ($r = 0.91$). Much of this correlation is due to the seasonal cycle, however, as the mean of all twelve monthly correlation coefficients equals 0.6. Figure 2 shows a scatterplot of individual rawinsonde launches versus the corresponding TOVS *PW* retrieval. Although there is strong correspondence between the measurements from the two instruments, the comparison shows a small but significant systematic difference. The slope of the least squaress linear regression is 0.83, and the mean of the rawinsonde *PW* divided by TOVS *PW* is 1.19, indicating that the TOVS *PW* retrievals are significantly lower than those from rawinsondes. This relationship is similar at all five retrieval levels.

[29] We suspect that clouds may play a role in explaining the apparent *PW* errors, as clouds are difficult to detect with

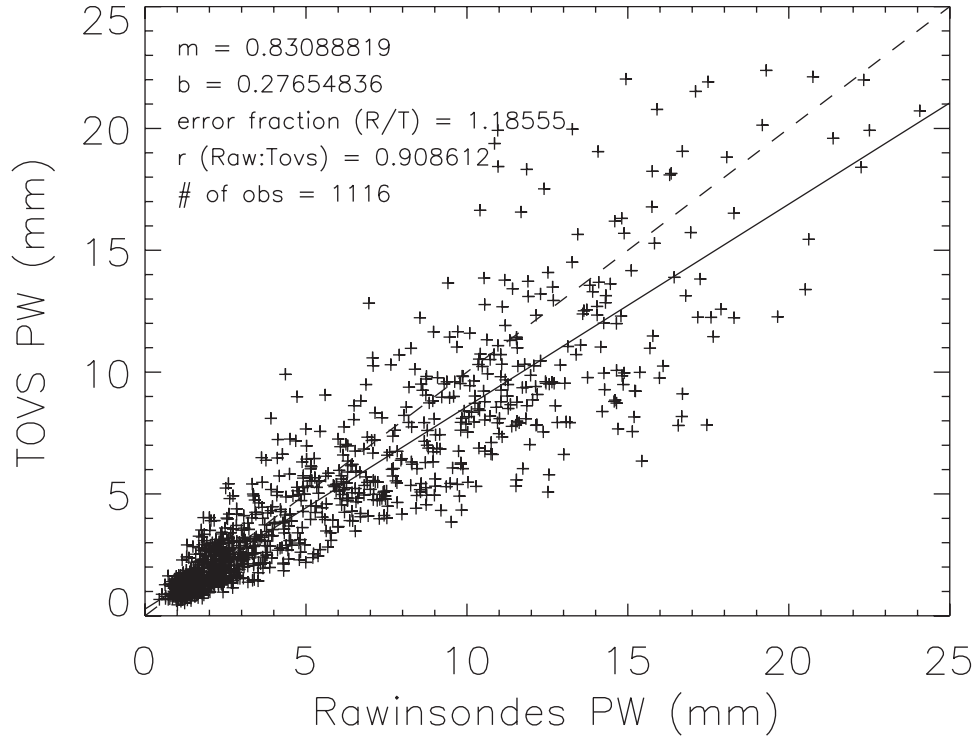

Figure 2. Scatterplot of NP rawinsonde and associated TOVS-derived total precipitable water. The solid line indicates the least squaress linear regression, and the dashed line indicates 1:1 correspondence.

passive satellite sensors over snow and ice. If clouds are not detected successfully in an early stage of the 3I algorithm, the resulting moisture profiles may be affected. *Schweiger et al.* [1999] compare TOVS/Path-P cloud fractions to conventional surface observations by humans. Correlations with surface-observed cloud fractions are strong, and retrievals successfully capture the annual cycle in the central Arctic. TOVS/Path-P estimates are shown to be superior to those from the International Satellite Cloud Climatology Project (ISCCP) [*Schweiger et al.*, 1999].

3.2.2. TOVS Precipitable Water Bias Identification and Correction

[30] The TOVS measurements and 3I retrieval algorithm have three deficiencies relevant to this study: (1) some remaining difficulty in distinguishing between low clouds and snow/sea ice, (2) inability to retrieve temperature and

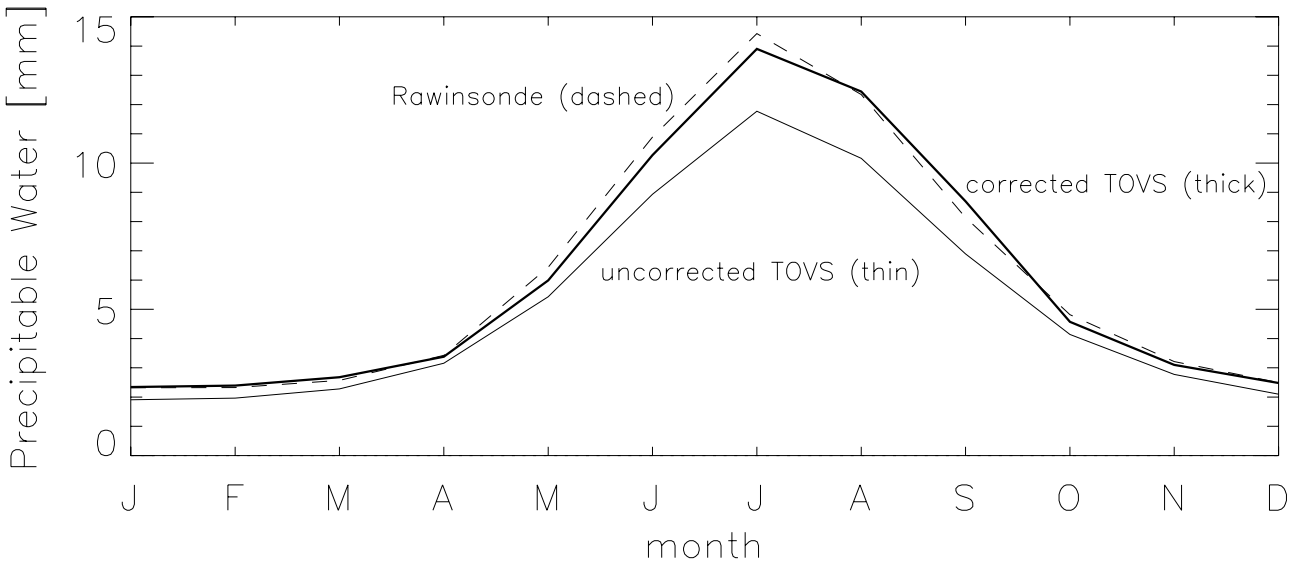

Figure 3. Annual cycle of precipitable water over the Arctic basin (as defined in Figure 7) for uncorrected Path-P TOVS retrievals (thin, solid), corrected TOVS retrievals (thick, solid), and gridded rawinsonde climatology (thin, dashed).

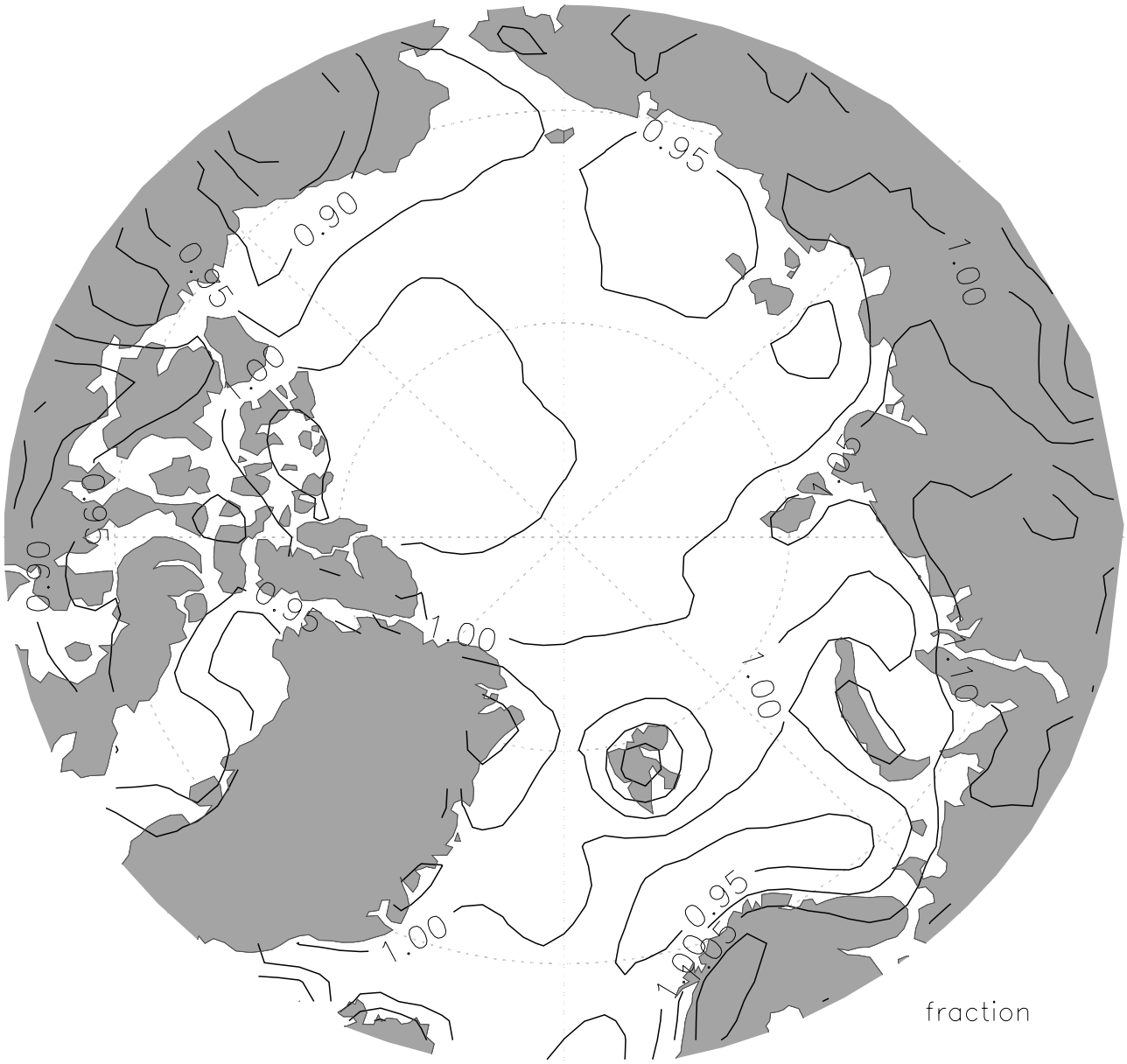

Figure 4. Ratio of annual mean total precipitable water from rawinsondes to corrected TOVS. The contour interval is 0.05.

PW profiles through heavy-overcast conditions, and (3) limitation to elevations below 1000 m in the present algorithm.

[31] *Francis* [1994] modified 3I's sea ice/cloud detection scheme and substantially reduced the retrieval errors caused by misidentification of cloudy and clear scenes over snow and sea ice. However, owing to limited availability at the time of validation data for calculating regression coefficients used in the schemes, errors still exist, as revealed by our comparisons of individual and monthly climatological TOVS *PW* with rawinsonde data.

[32] The algorithm to retrieve deep-layer moisture content performs poorly in heavy-overcast conditions. If the retrieved "effective cloud fraction" (cloud cover multiplied by the cloud emissivity) in a retrieval box is less than 60%, a cloud-clearing method using pairs of HIRS and MSU channels removes the effects of clouds on the moisture-sensitive HIRS channels. When the retrieved cloud cover exceeds 90%, the 3I algorithm cannot retrieve *PW* profiles. These conditions tend to occur in deep cloud systems, which are often precipitation producers. While cloud cover in the Arctic is high year-round, clouds are often relatively thin, and thus *PW* profiles can be retrieved in all but a small fraction of cases. We have developed an empirical method to correct the *PW* retrievals in these cases. Finally, retrievals are also not performed over elevations exceeding 1000 m, thus we exclude retrievals in Greenland and continental mountain ranges.

[33] In an effort to produce the most accurate fields of *PW* possible, we combine the best attributes of rawinsonde measurements and TOVS retrievals. Rawinsonde data provide excellent climatologies of *PW* with high vertical

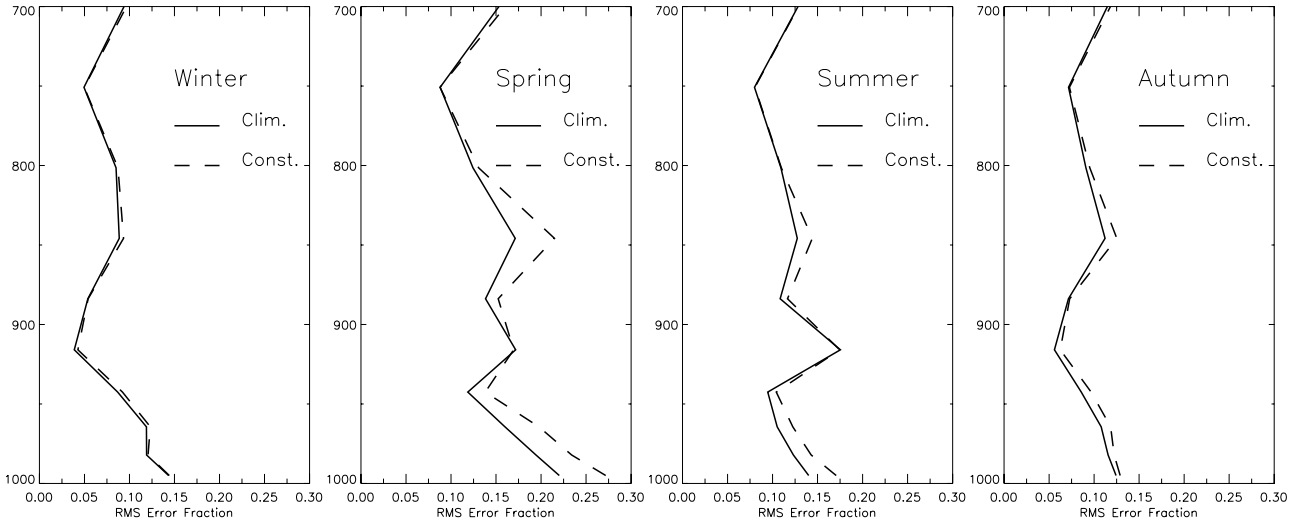

Figure 5. Root-mean square-error fraction in corrected seasonal mean profiles of relative humidity as compared to *RH* profiles directly from rawinsondes. The solid line compares the corrected *RH* vertical distribution using TOVS *PW* and temperature retrievals with monthly climatological *RH* profiles, and the dashed line is the same but using a constant climatological *RH* profile.

resolution, but much of the Arctic is void of rawinsonde stations. The TOVS retrievals, in contrast, provide excellent spatial and temporal coverage, yet lack vertical resolution. We use rawinsonde data, which have been carefully screened according to *Serreze et al.* [1994], to "calibrate" the TOVS *PW* retrievals to the rawinsonde climatology. The annual cycle of the resulting correction factors over the central Arctic range from 3 mm in the summer to less than 1 mm in the winter, or less than 10% in April and November to approximately 20% in January and September (Figure 3).

[34] We find that the primary reasons for the corrections are different over sea ice, open ocean, and land. Cloudiness explains 79% of the annual error fraction variance over sea ice, revealed by comparing data from each NP rawinsonde launch with the nearest TOVS *PW* retrieval and TOVS retrieved cloud fraction. From July through September, when cloud and moisture amounts are largest, cloud cover explains 84% of the binned fractional error (bin width of 10%). During the summer the *PW* error ranges from 5% for samples in the 5% cloud-cover bin to over 35% for samples in the 95% bin. This relationship is strong for all months except March and April. Over open ocean there is no significant relationship between cloudiness and the *PW* fractional error because clouds are relatively easy to detect over open water. The fractional error varies between 1.03 and 1.20 over the annual cycle, as revealed by comparisons of TOVS retrievals with individual rawinsonde launches from the NCEP Marine Archive. Over land, a regression of the annual climatological *PW* fractional error versus elevation at each of the permanent land stations (located below 1000 m elevation) shows that elevation explains 41% of the fractional error. Errors over high elevation are greatest during fall and winter, and least during spring, probably resulting from pooling of cold, moist air in valleys, large horizontal variability, and very cold temperatures that approach the sensitivity limits of some HIRS channels. At sea level, the error fraction is very similar to that computed over open water regions. The correlation between cloud fraction and *PW* errors over land is insignificant. Finally, *Elliot and Gaffen* [1991] report biases in rawinsonde water vapor measurements at extremely cold temperatures, which may contribute to the difference between TOVS *PW* and measured values. These conditions occur primarily over land in winter and the moisture content is extremely small, consequently the impact on moisture transport and *PW* convergence over the Arctic Ocean is also small.

[35] We multiply the original TOVS *PW* by an empirically derived, time-varying correction factor to yield values that agree more closely with rawinsonde measurements. Fractional correction values are used instead of standard linear regression coefficients in order to weight the fractional error equally among high *PW* and low *PW* conditions. Over sea ice we use correction coefficients based on the computed time-varying, climatological relationship between the *PW* error and cloud fraction. Over open water the correction coefficient varies only over the annual cycle. Over land, monthly regression coefficients are computed by minimizing the squared error for the fractional error (Q_{raw}/Q_{TOVS}) versus elevation.

[36] Daily correction coefficients are interpolated from monthly coefficients and applied to all TOVS precipitable water data according to surface type (sea ice, open water, or land). Using this technique, fractional error is reduced from an average of 1.18 to 0.98 over the Arctic basin (Figure 4). Over land, errors have also been reduced considerably, although at the higher elevations they are still large (greater than 1.10). The TOVS data are slightly over-corrected over the Canadian Archipelago and off the coast of Alaska and Canada. Figure 3 shows the monthly mean error fraction over the Arctic basin before and after the correction.

[37] During the non-summer months over the ice pack, strong near-surface temperature inversions are usually associated with sharp vertical gradients in the moisture profile and frequently support strong vertical wind shear. Because the TOVS precipitable water retrievals are thick-layer averages (five layers between the surface and 300 hPa),

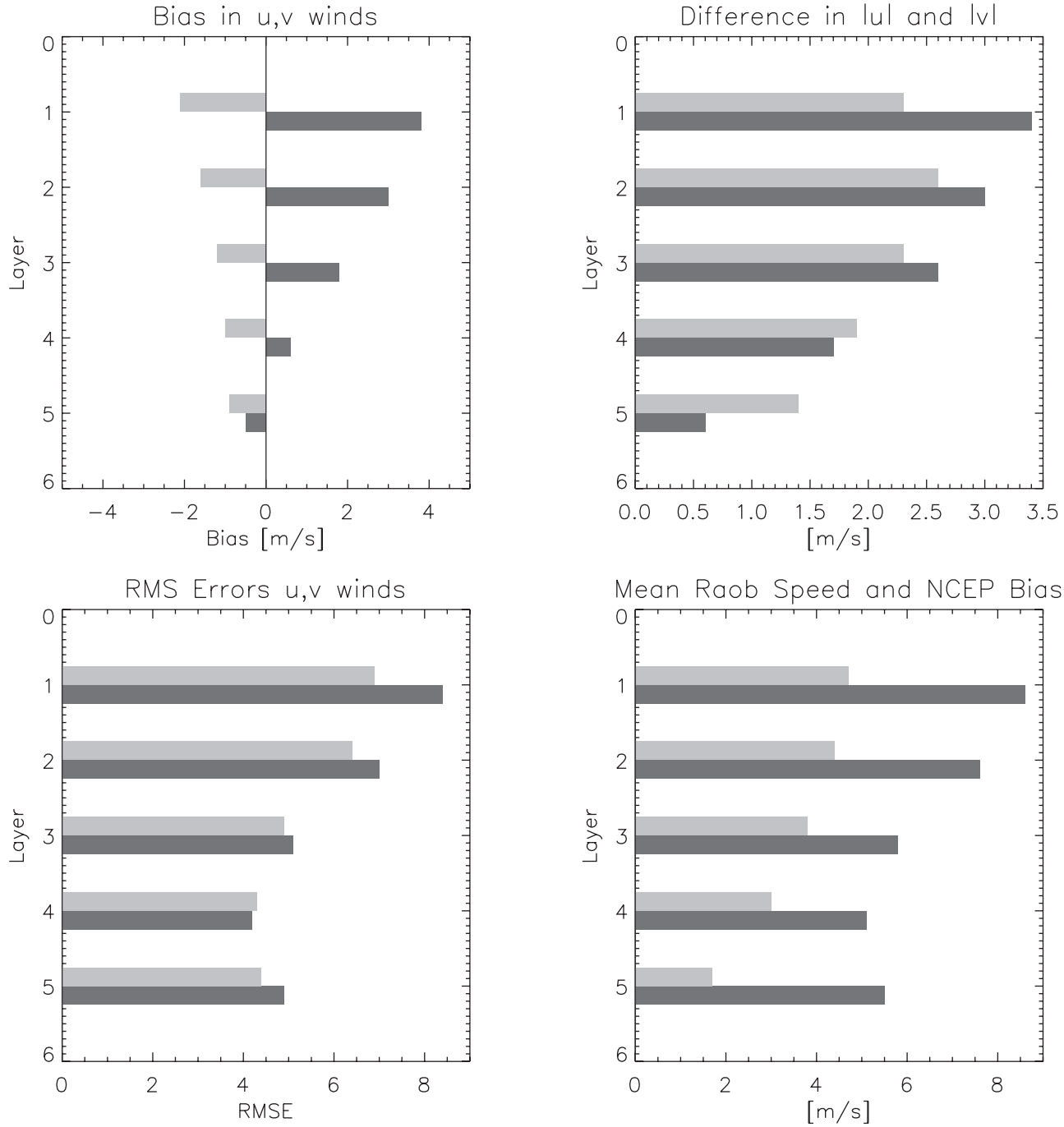

Figure 6. Comparison of NCEP-NCAR Reanalysis upper-level winds to measurements by rawinsondes during the CEAREX and LeadEx Arctic field programs. Layers 1 through 5 are bounded by the following pressure levels: 300, 400, 500, 700, 850, and 1000 hPa. The *u* wind is dark gray and *v* is light gray. (a) The bias in *u* and *v*; (b) the difference in mean absolute magnitudes of *u* and *v* (NCEP-rawinsonde); (c) RMS errors in *u* and *v*; (d) the mean wind magnitude from rawinsondes and bias in the NCEP-NCAR speed.

a method is needed to distribute the moisture realistically within the layer. While the lowest TOVS precipitable water layer is 150 hPa thick, the TOVS temperature retrievals have higher vertical resolution (eight levels between the surface and 300 hPa), and capture near-surface temperature inversions. We exploit the higher resolution temperature retrievals along with time-varying, climatological *RH* profiles from rawinsondes to enhance the vertical resolution of the *PW* retrievals. Summarizing this procedure, which is described completely in *Groves* [2001], the TOVS temperature retrievals and climatological relative humidity profiles from rawinsondes are first combined to create *PW* profiles. These new *PW* profiles are then scaled within each deep TOVS *PW* layer so the total *PW* in the new profile equals

Figure 7. Definitions of Arctic Ocean regions used throughout the text. "Arctic basin" refers to regions 1–7.

that of each retrieved TOVS *PW* layer. Consequently, daily variations in *RH* profiles, particularly during precipitation events, will be captured in retrieved temperature and redistributed *PW* fields, thereby producing final profiles that represent much of the small time- and space-scale variability. Figure 5 compares this *PW* distribution scheme to one assuming constant relative humidity, and shows that it successfully distributes *PW* within the thick retrieval layers, with small errors in the final seasonal mean specific humidity profiles. Missing pixels in the TOVS precipitable water fields are linearly interpolated on each sigma level from the nearest neighbors prior to computing the moisture budget.

3.3. NCEP-NCAR Reanalysis Wind Fields

[38] We use daily surface pressure and upper-level winds for 12 UTC (to correspond to the daily average TOVS retrievals) from the NCEP-NCAR reanalysis data set. The wind fields are provided on a $2.5^\circ \times 2.5^\circ$ grid at 28 sigma levels and were obtained directly from NCAR. We use only the bottom 16 levels that lie between the surface and 300 hPa and optimally interpolate onto the $(100\ \text{km})^2$ EASE grid. Distances between NCEP-NCAR and EASE grid points are relatively small, thus errors resulting from the interpolation should be negligible. While NCEP-NCAR Reanalysis *PW* products have been shown to contain significant errors over the data-sparse Arctic, we have greater confidence in the accuracy of the wind fields. In addition, there is no superior source of wind data for the Arctic region at this time, as other reanalyses suffer from the same data sparsity. According to observation counts available on the NCEP-NCAR Reanalysis website, some satellite-derived temperatures are assimilated over the Arctic, although many

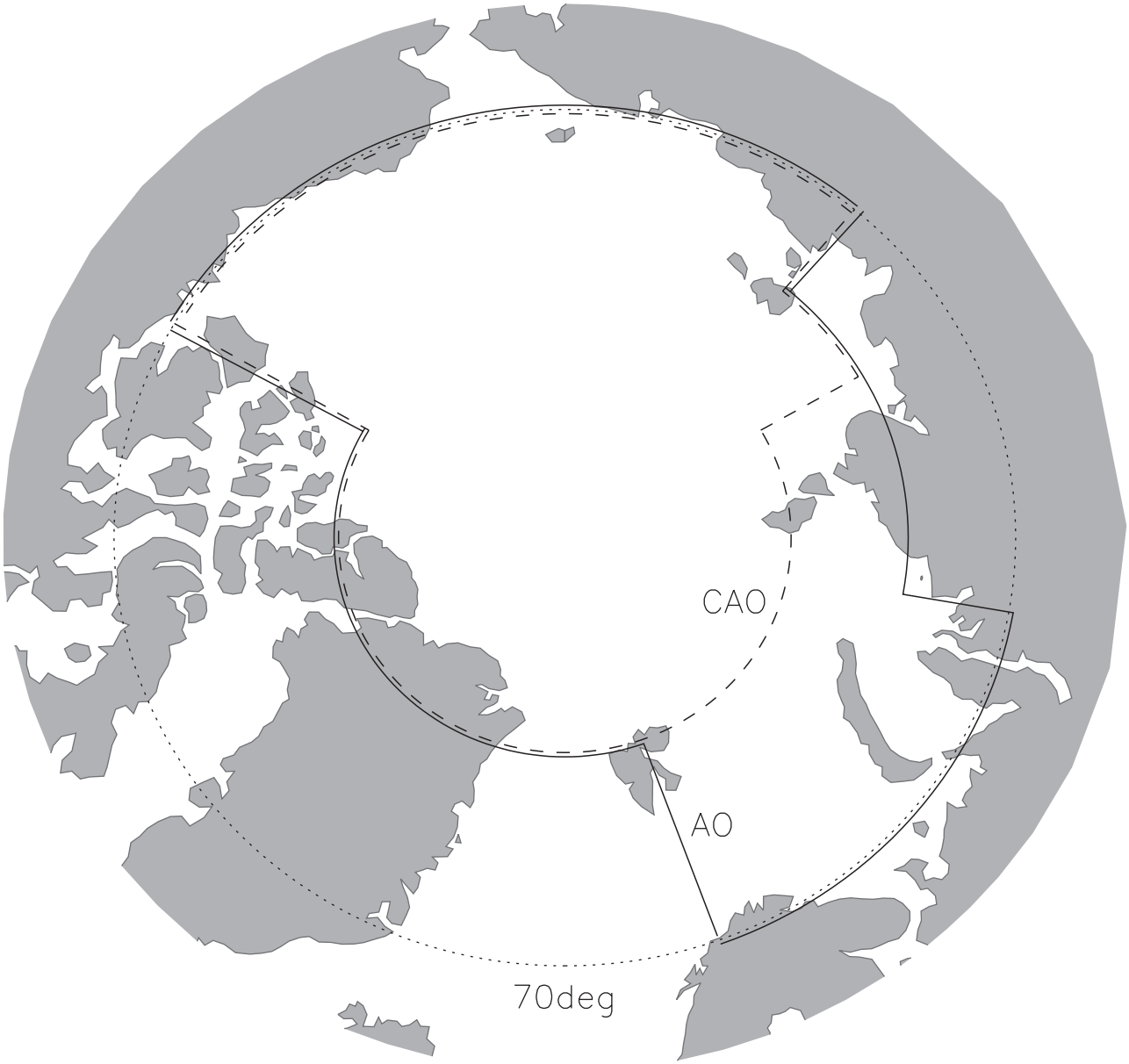

Figure 8. Definitions of Arctic regions from *Serreze and Barry* [2000]: Central Arctic Ocean (CAO, dashed), Arctic Ocean (AO, solid), and Polar Cap (70°N, dotted).

fewer per gridbox than in lower latitudes. These temperatures, along with surface pressure data from buoys on the sea ice, aid in diagnosing the upper-level height and wind fields. In contrast, the reanalysis does not assimilate moisture information from satellites over the Arctic, and moreover *PW* is influenced by a variety of complex processes, such as evaporation, condensation, and sublimation both at the surface and in clouds. Consequently, the use of NCEP-NCAR wind fields is justified, while TOVS *PW* fields represent a substantial improvement over *PW* from reanalyses.

[39] Validation of reanalysis upper-level winds is difficult owing to the lack of independent data, as the reanalyses assimilate as many rawinsonde measurements as possible. By obtaining the actual data record of the time, latitude, and longitude of rawinsondes that were assimilated by the NCEP reanalyses, we were able to confirm that rawinsondes from the Coordinated Eastern Arctic Experiment (CEAREX) and the LeadEx field programs were not in the database. CEAREX was conducted from a ship in the Arctic Ocean northeast of Spitsbergen from September to

Table 1. Areas (in 10^6 km^2) of Each Region Shown in Figures 7 and 8[a]

Region	Area	Region	Area
Beaufort Sea (1)	0.92	Nansen Basin (7)	0.53
Chukchi Sea (2)	1.25	Kara and Barents seas (8)	2.11
Canada Basin (3)	0.71	GIN seas (9)	2.17
Central Arctic (4)	0.45	Central Arctic Ocean (CAO)	15.30
Laptev Sea (5)	1.52	Arctic Ocean (AO)	9.77
North Pole (6)	1.40	Polar Cap (70°N)	7.31

[a] Note that regions 1–9 exclude land.

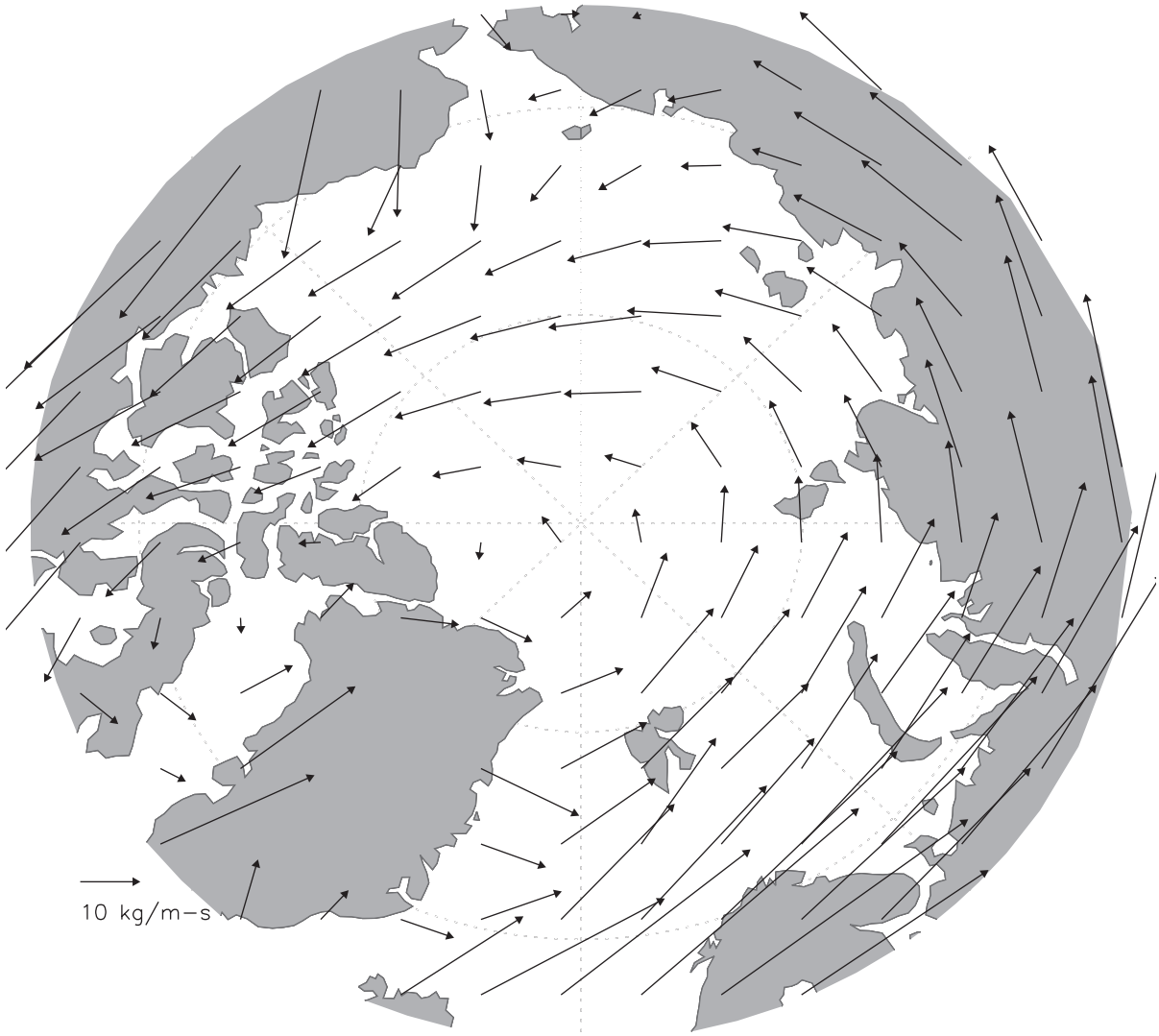

Figure 9. Annual mean precipitable water flux vectors derived from TOVS *PW* profiles and NCEP-NCAR upper-level winds (1980–1993).

December, 1988, and LeadEx took place in the Beaufort Sea in Spring, 1992. We interpolate spatially the nearest four reanalysis grid points within 2 hours of the launch to each rawinsonde location to obtain a set of approximately 380 collocations. Mean-layer winds are evaluated in 5 layers bounded by the following pressure levels: 1000, 850, 700, 500, 400, and 300 hPa. Because both field programs were located relatively near a coast where routine rawinsondes are launched, we expect that the validation results shown here exhibit smaller errors than those existing in the central Arctic Ocean, farther from assimilated data.

[40] Figure 6 presents summary statistics for the validation of NCEP Reanalysis winds with independent CEAREX and LeadEx rawinsonde data. Biases in the u and v components (Figure 6a) show that NCEP winds are generally too westerly (u component too positive) and too northerly (v component too negative), which would contribute to a negative bias in *PW* flux convergence into the Arctic basin. While values appear relatively small, they represent a large percentage error compared to the mean values (Figure 6d). We also examined ECMWF Reanalysis (ERA) winds and found similar errors. See *Francis* [2002] for further details of this validation study. Although these findings are somewhat discouraging, we use the NCEP-NCAR upper-level winds for lack of a better source of wind data and note that uncertainties may vary spatially in the basin relative to semi-permanent circulation features.

4. Methodology

[41] To estimate the *PW* flux between the atmosphere and the ice/ocean surface (net precipitation), we use a quasi-horizontal finite difference scheme to evaluate the moisture budget daily at each horizontal grid point of the Path-P EASE grid and at 16 verticals levels. The summation of each layer's moisture budget (equations (3) and (4)) yields net precipitation, $(P\text{-}E)_{\mathrm{calc}}$.

[42] Each daily $(P\text{-}E)_{\mathrm{calc}}$ field comprises the true daily convergence plus an error term owing to the finite-differencing scheme. This error averages out on the order of 3 days, and consequently the subsynoptic-scale noise produced by the finite difference scheme is minimized by smoothing fields

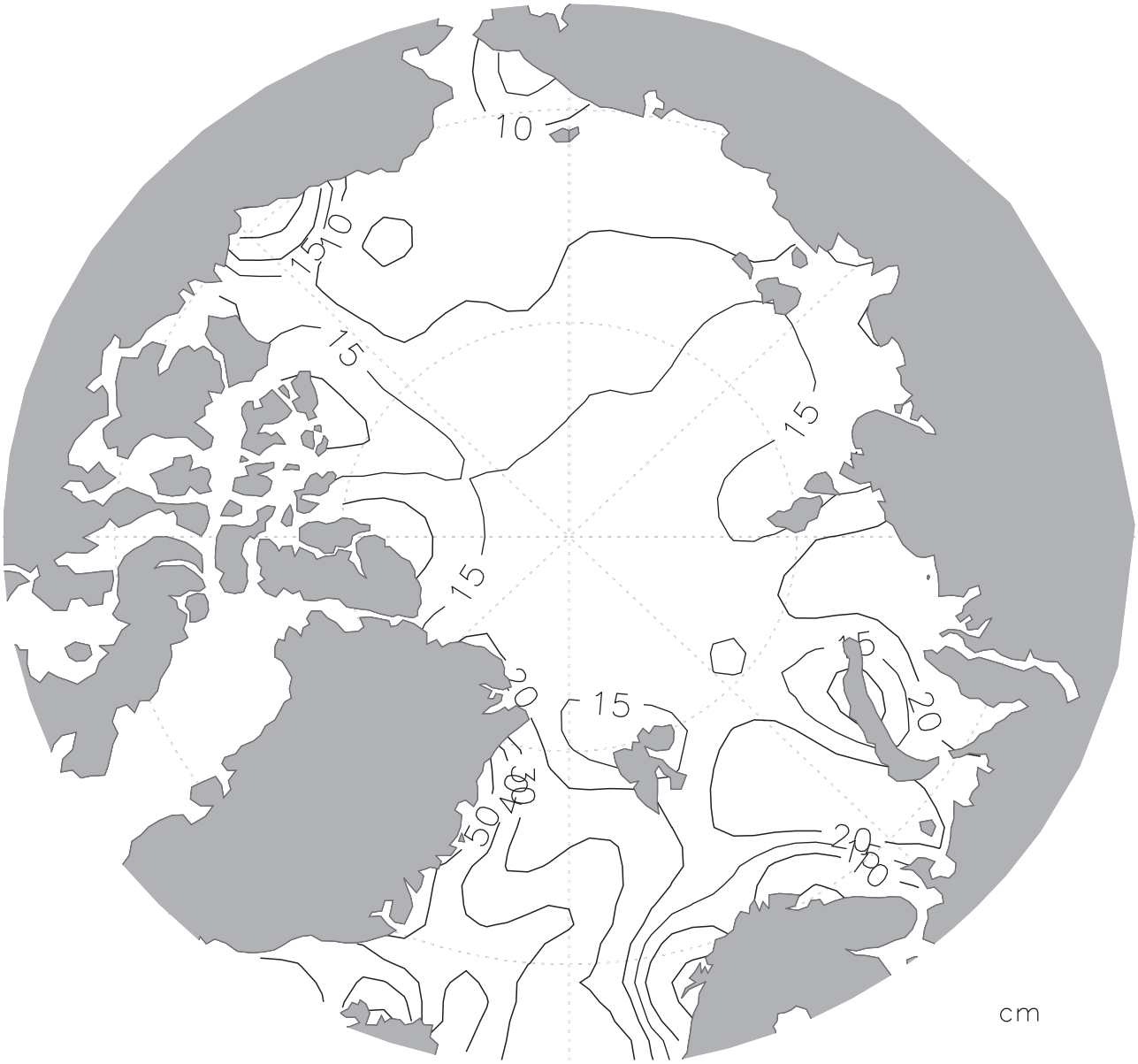

Figure 10. Annual precipitable water flux convergence (cm yr^{-1}) from TOVS *PW* and NCEP-NCAR winds (1980–1993). Contour interval is 10 cm yr^{-1} (thick) with the 15 cm yr^{-1} added (thin).

of $(P\text{-}E)_{calc}$ in space and time with a 5 × 5 grid-box and a 5-day running-mean filter. Note that only the $(P\text{-}E)_{calc}$ product is smoothed.

[43] The monthly mean daily *PW* flux, $\langle Q\vec{V}\rangle$, and *PW* flux convergence, $-\nabla\cdot(\langle Q\vec{V}\rangle)$, can be decomposed into two components. The first is calculated from monthly mean wind and *PW* fields, and represents the inter-monthly and inter-annual variability (*b*). The second is the high-frequency transient component that represents intramonthly variability (*c*):

$$\underset{a}{\langle Q\vec{V}\rangle} = \underset{b}{\langle Q\rangle\langle\vec{V}\rangle} + \underset{c}{\langle Q'\vec{V}'\rangle} \tag{5}$$

$$\underset{a}{-\nabla\cdot\left(\langle Q\vec{V}\rangle\right)} = \underset{b}{-\nabla\cdot\left(\langle Q\rangle\langle\vec{V}\rangle\right)} \underset{c}{-\nabla\cdot\left(\langle Q'\vec{V}'\rangle\right)} \tag{6}$$

where the brackets, $\langle\ \rangle$, signify monthly means, and the primes indicate daily anomalies from the monthly means. The covariance terms $\langle\langle Q\rangle\vec{V}'\rangle$ and $\langle Q'\langle\vec{V}\rangle\rangle$ equal zero in this decomposition and have been removed from Equations 3 and 4.

[44] We compute *PW* flux and *PW* flux convergence using monthly *PW* and wind data (terms labeled *b*). Subtracting these fields from monthly means of the daily *PW* flux and *PW* flux convergence (*a* terms) yield the high frequency transient terms (*c* terms). Hereafter we refer to (*a*) terms as the total *PW* flux and total *PW* flux convergence, (*b*) terms as the inter-monthly mean components of the total, and (*c*) terms as high-frequency transient components of the total.

[45] To describe the moisture budget we show individual budget terms as a function of space and averaged over different regions in the Arctic. Figure 7 shows the nine

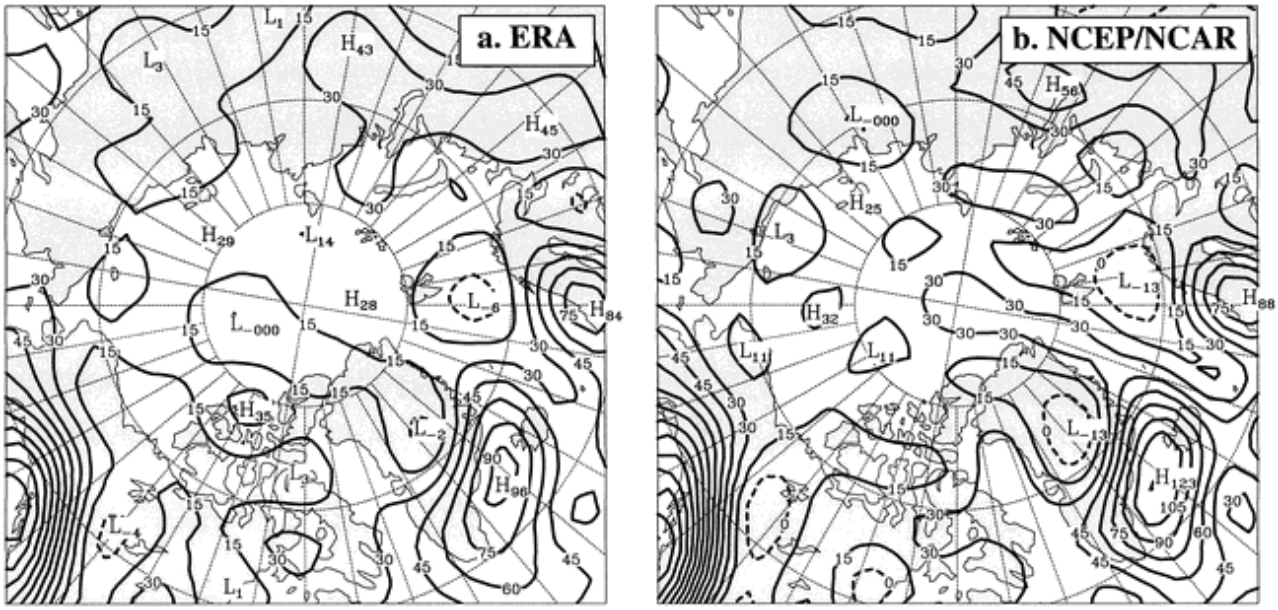

Figure 11. As in Figure 10 but from (a) ERA and (b) NCEP reanalyses for 1979 to 1993 [from *Cullather et al.*, 2000]. Contour interval is 15 cm yr^{-1}.

Arctic and North Atlantic regions, consistent with those defined in previous studies of the Arctic Ocean freshwater budget [*Steele et al.*, 1996]. These regions are indexed numerically. To compare TOVS calculations to others in the literature, we also use a set of boundaries defined primarily by latitude and longitude as shown in Figure 8. Table 1 lists the area of each region in Figures 7 and 8.

5. Results

5.1. Annual Means

[46] The climatological (1980 to 1998) annual mean field of total *PW* flux from TOVS, $\vec{F}$, is dominated by cyclonic and mainly zonal moisture transport centered just poleward of Greenland (Figure 9). Moisture enters the Arctic primarily over the GIN and Chukchi Seas and exits over the Canadian Archipelago, agreeing with prior moisture transport studies. This cyclonic transport is opposite to the anti-cyclonic mean low-level winds associated with the Beaufort Gyre.

[47] The corresponding climatological annual mean *PW* flux convergence, $\left(-\nabla \cdot \vec{F}\right)/\rho_w$, from TOVS is greatest over regions of large poleward flux: over the GIN, Barents, and Chukchi Seas (Figure 10). Over the Eurasian/Atlantic sector of the Arctic Ocean, flux convergence exceeds 15 cm yr^{-1} and decreases to ~10 cm yr^{-1} over the Beaufort Sea. A local minimum exists just north of Alaska.

[48] The pattern of climatological annual flux convergence derived from NCEP-NCAR and ECMWF reanalyses (Figure 11) from 1979 to 1993 [*Cullather et al.*, 2000] is similar to the TOVS field, especially in regions where rawinsonde data are available, but differs significantly over much of the central Arctic Ocean where conventional data are sparse. This comparison gives further credibility to TOVS-derived moisture values and offers additional evidence that reanalysis values in data-sparse areas are of questionable accuracy. Most major features are found in both results, including strong convergence over the GIN and Kara Seas, and convergence greater than 15 cm yr^{-1} over the Eurasian/Atlantic oceanic sector. A local minimum over the Canadian sector is also present in the reanalysis data (although it is slightly poleward of the TOVS minimum). The ERA data, however, show higher values over the Nansen Basin (28 cm yr^{-1}) and Chukchi (29 cm yr^{-1}) Seas. The analogous field from NCEP-NCAR data is considerably noisier than either the TOVS or ERA fields and has higher values throughout [*Cullather et al.*, 2000]. The TOVS field does not have the region of negative convergence south of Svalbard that is evident in both reanalyses. *Serreze and Hurst* [2000] find that both reanalyses underestimate precipitation in the Atlantic region of the Arctic and that the NCEP-NCAR significantly overestimates evaporation, which suggests that the TOVS-derived pattern is more realistic.

Table 2. Annual Climatological Precipitable Water Flux Convergence $\left(-\nabla \cdot \vec{F}\right)/\rho_w$ From TOVS (This Study), ERA and NCEP-NCAR Reanalysis Data [*Bromwich et al.*, 2000], and Three Estimates From Rawinsondes[a]

	Polar Cap	Arctic Ocean	Central Arctic Ocean
TOVS	15.1	14.5	13.4
ERA	18.2	17.9	16.5
NCEP-NCAR	19.4	19.5	19.3
Serreze and Barry [2000]	16.1	15.3	17.4
Nakamura and Oort [1988]	11.7	–	–
Masuda [1990]	14.8	–	–
ERA $(P\text{-}E)_{fcst}$	13.2	13.3	12.7
NCEP-NCAR $(P\text{-}E)_{fcst}$	11.2	10.5	11.9
Masuda [1990] $(P\text{-}E)_{calc}$	15.5	–	–

[a] Also tabulated are the forecast *P* minus forecast *E* estimates from both reanalysis data sets [*Bromwich et al.*, 2000] and *P-E* calculated from rawinsonde data. Domains are shown in Figure 8. Units are cm yr^{-1}.

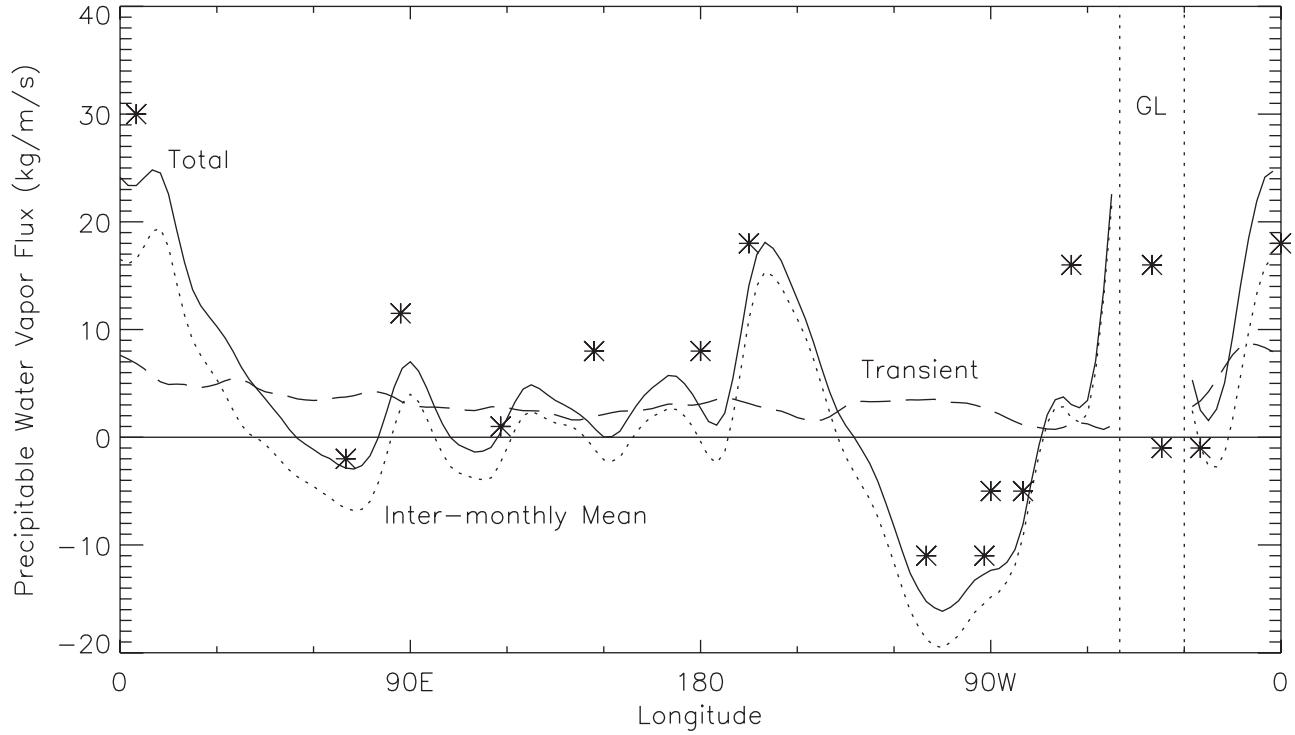

Figure 12. Components of TOVS-derived total meridional vapor flux across 70°N in kg m^{-1} s^{-1}: total (solid), inter-monthly mean (dotted), and transient (dashed). For reference, asterisks represent select values from the rawinsonde data shown in Figure 13.

[49] Table 2 summarizes the annual *PW* flux convergence estimates using TOVS, rawinsonde, ERA, and NCEP-NCAR reanalysis data. Also included are forecast *P* minus forecast *E* values from the two reanalysis data sets and two estimates of *P-E* calculated from rawinsonde data. Recall that annual-mean *PW* flux convergence is equivalent to annual net precipitation. All values are computed for nearly the same 14-year time period (1979 to 1993) except that TOVS data begin in October 1979, those from *Nakamura and Oort* [1988] are for 1963 to 1973, and *Masuda* [1990] is for only one year (Dec. 1978 to Nov. 1979). Estimates of $\left(-\nabla \cdot \vec{F}\right)/\rho_w$ over the entire polar cap (poleward of 70°N) range from 11.7 cm yr^{-1} [*Nakamura and Oort*, 1988] to 19.4 cm yr^{-1} (NCEP-NCAR).

[50] The TOVS estimate is 94% of the rawinsonde estimate and 83% of the ERA estimate overall. Over the Arctic Ocean region, the TOVS and rawinsonde estimates are very close (the TOVS estimate is 95% of the rawinsonde estimate). Over the Central Arctic Ocean domain the TOVS estimate is considerably lower than the others. This is due to lower calculated *PW* flux convergence in the Western/Pacific sector of the Arctic Ocean. We examine causes for this discrepancy in the following section. Finally, as discussed in section 2.3, both ERA and NCEP-NCAR forecast *P-E* estimates are significantly lower than all the convergence estimates.

[51] To better understand the differences between the TOVS-derived values and others, we examine the longitudinal variability of the *PW* flux across 70°N from TOVS, rawinsonde, and reanalysis data (Figures 12 and 13). The total meridional *PW* flux from rawinsonde, ERA, and NCEP-NCAR reanalysis data exhibit a similar pattern to those from TOVS. The rawinsonde data contain a stair-step pattern, reflecting the method used to interpolate data from fixed rawinsonde stations, whereas the TOVS and reanalysis estimates show more realistic peaks and troughs in vapor flux than the rawinsonde estimate, as discussed by *Bromwich et al.* [2000]. In eastern longitudes the pattern and magnitudes in the meridional flux from TOVS closely resembles that from the ERA. The TOVS *PW* transport peaks in the North Atlantic at about 23 kg m^{-1} s^{-1}, slightly higher than the ERA estimate, but with a similar double

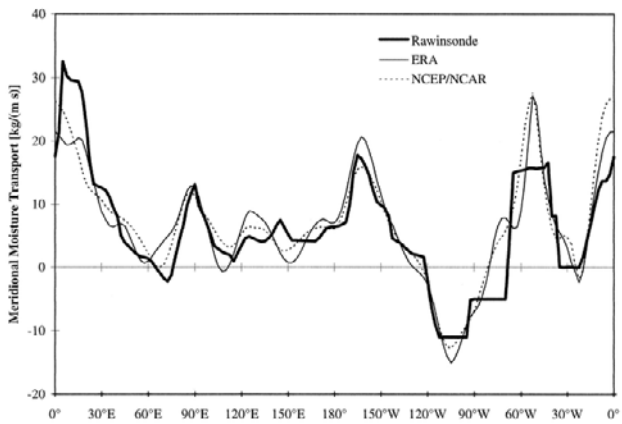

Figure 13. Total meridional vapor flux across 70°N from rawinsonde data, ERA, and NCEP-NCAR Reanalysis data, from 1979–1993 in kg m^{-1} s^{-1}. From *Cullather et al.* [2000].

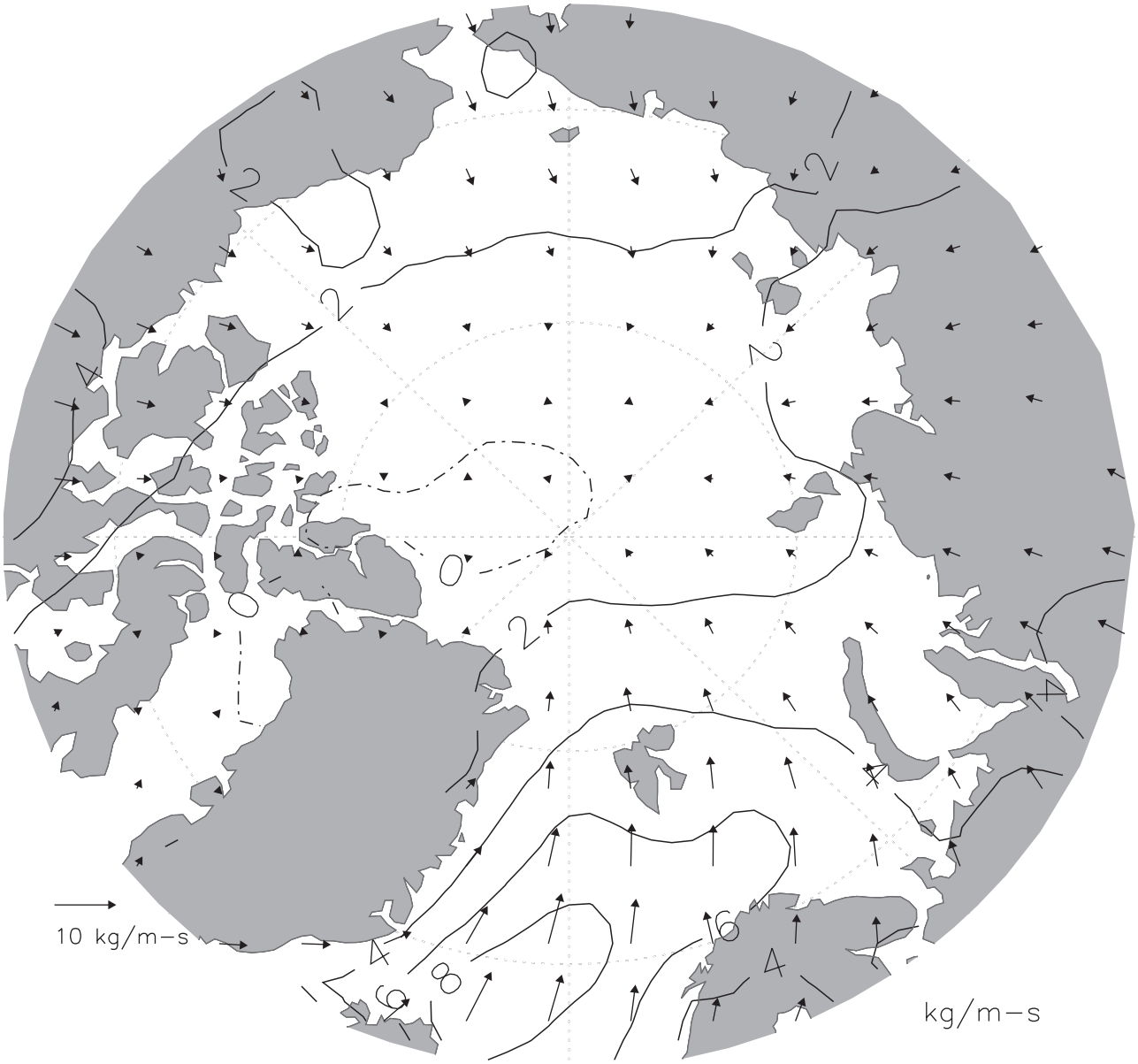

Figure 14. Vectors of annual high-frequency transient precipitable water flux and magnitude of meridional component (contours) for 1980–1998 from TOVS. Contour interval is 2 kg m^{-1} s^{-1}.

peak. The TOVS meridional fluxes between 60°E and the date line show a wave-like structure similar to both reanalysis data sets. Smaller poleward flux in the east and larger equatorward flux in the west derived from TOVS data explain much of the annual difference between the TOVS flux convergence and other estimates shown in Table 2. The lack of data, both TOVS retrievals and rawinsondes, over Greenland is also a likely source of discrepancy. The exclusion of any part of the "wall" across 70°N is likely to contribute to differences among data sets, as well, especially near Greenland where transports are large and highly variable in space and time. Because the wind fields we used are the same as those used for the NCEP-NCAR calculations, differences in fluxes between TOVS and NCEP must result from differing moisture amounts in the data sets.

Table 3. Total, Stationary Mean, and Transient Eddy Contributions to the TOVS Annual Precipitable Water Flux Convergence Over the Regions Shown in Figure 7[a]

Region	Precipitable Water Flux Convergence, cm yr^{-1}		
	Total	Stationary Mean	Transient Eddy
Beaufort Sea (1)	11.0	2.6 (24%)	8.5 (76%)
Chukchi Sea (2)	9.0	2.1 (23%)	7.0 (77%)
Canada Basin (3)	12.7	3.5 (28%)	9.2 (72%)
Central Arctic (4)	13.0	4.0 (31%)	9.0 (69%)
Laptev Sea (5)	13.3	3.4 (26%)	9.9 (74%)
North Pole (6)	15.8	5.1 (32%)	10.8 (68%)
Nansen Basin (7)	16.2	1.7 (10%)	14.5 (90%)
Kara and Barents seas (8)	17.8	6.3 (35%)	11.4 (65%)
GIN seas (9)	24.1	16.5 (68%)	15.8 (32%)
Arctic Basin (1–7)	12.9	3.3 (26%)	9.6 (74%)

[a] Units are cm yr^{-1}. Values in parentheses are percentages of the total.

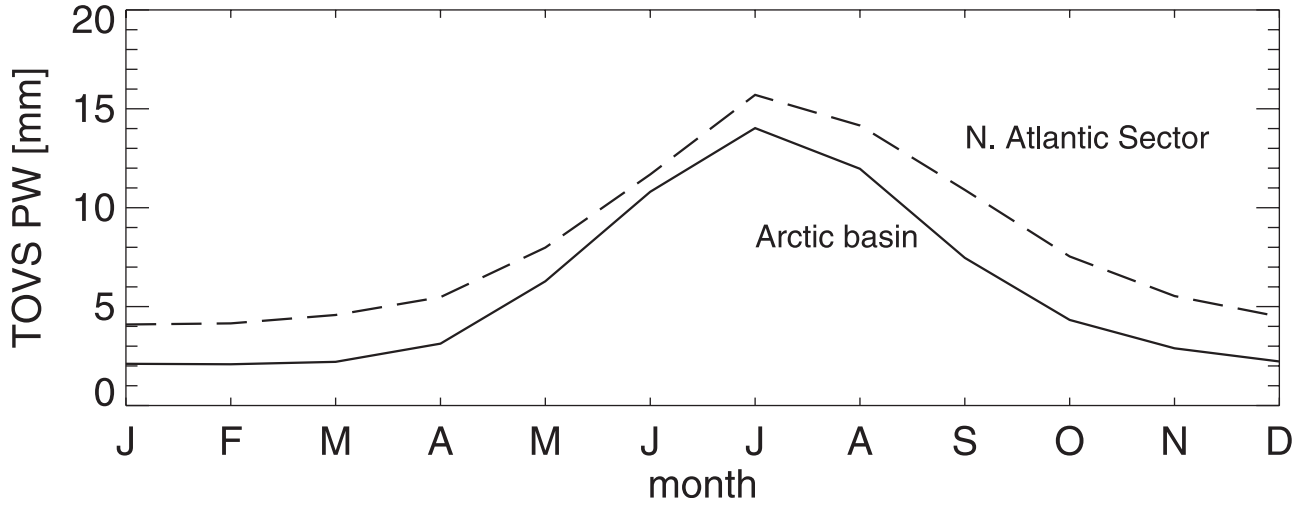

Figure 15. Annual cycle of precipitable water over the Arctic Basin (regions 1–7) and the North Atlantic sector (regions 8–9) from TOVS.

[52] Figure 12 identifies more clearly the major pathways of moisture transport into the Arctic shown in the annual *PW* flux field (Figure 9): the North Atlantic (around the prime meridian), over northwestern Alaska (centered around 150°W), and around the western side of the Greenland continent (between 30°W and 50°W). There is also moderate poleward vapor transport over northern Asia between 90°E and the date line. Finally, moisture exits over the Canadian Archipelago (between 75°W and 130°W). Note that the integration of the total meridional *PW* flux curve is proportional to the total *PW* flux convergence poleward of 70°N.

[53] To characterize the temporal scale of the moisture transport and deposition, we show the high-frequency transient component of the annual mean *PW* flux (Figure 14), which is the difference between the total *PW* flux (Figure 9) and the inter-monthly mean component (computed from daily and monthly data; not shown). The transient contribution is always poleward and very small except over the GIN and Barents Seas, where it exceeds 4 kg m^{-1} s^{-1}. Even though the magnitude of the transient flux is a small fraction of the total mean flux (Figure 12), the poleward transport by transients contributes the majority of poleward transport over the Barents and Kara Seas and western portion of the GIN Seas (Table 3). The inter-monthly mean *PW* flux (not shown) dominates the total over the rest of the Arctic.

[54] In contrast to the *PW* flux, the *PW* flux convergence over the Arctic Ocean is dominated by high-frequency transient eddies. Over the Arctic basin, the transient flux convergence accounts for about three fourths of the total convergence (Table 3). Transients contribute more than 65% of the total flux convergence over all regions except for the GIN seas, where the inter-monthly mean field is about 70% of the total flux convergence field.

5.2. Annual Cycles

[55] To better understand the annual cycle of the moisture budget, we evaluate the annual cycles of key parameters-total precipitable water (*PW*), lower-troposphere winds, *PW* flux, and *PW* flux convergence (*P-E*).

[56] Between November and March, the central Arctic atmosphere is cold and extremely dry, containing less than 3 mm of *PW*. Summertime *PW* is about five times higher, peaking at about 14 mm in July (Figure 15). Over the North Atlantic sector, the winter *PW* amounts are ~5 mm, which is twice as high as those over the central Arctic. The July *PW* exceeds 15 mm over the GIN Seas.

[57] To compare the TOVS annual cycle of *PW* flux with other estimates, we plot the annual cycle of the monthly mean meridional *PW* flux across 70°N from TOVS, rawinsondes, ERA, and NCEP-NCAR reanalysis data (Figure 16). The TOVS poleward *PW* transport across 70°N is less than 5 kg m^{-1} s^{-1} between October and March and exceeds 7 kg m^{-1} s^{-1} during June and August. The annual cycle of rawinsonde poleward vapor transport from *Cullather et al.* [2000] is very similar to the TOVS estimate, although the TOVS meridional flux is significantly lower during September and October. Rawinsonde-derived values from *Nakamura and Oort* [1988] are lower than all other estimates except in fall. Both reanalysis data sets show 20 to 30% greater poleward moisture transport during June–September.

[58] *Cullather et al.* [2000] suggest that the reanalysis estimates of total *PW* flux at 70°N are likely to be more accurate than the rawinsonde estimates because the differences are primarily due to discrepancies over a narrow longitudinal range (40°W to 60°W) during years when an important rawinsonde station is missing. Of course, missing rawinsondes also impact the reanalysis data by not being available for assimilation, and the TOVS values are affected by missing retrievals over high elevation, particularly over Greenland. *Cullather et al.* [2000] contend that reanalysis models should be able to more realistically interpolate across regions lacking assimilation data. The question remains, however, what biases exist in reanalysis *PW* values over regions lacking assimilation data. As noted section 2, *Bromwich et al.* [2000] show large summertime NCEP-NCAR *PW* errors over the central Arctic (based on comparisons with data from Russian drifting station NP 28). If the reanalysis values are erroneously low, as suggested by the comparisons, flux convergence

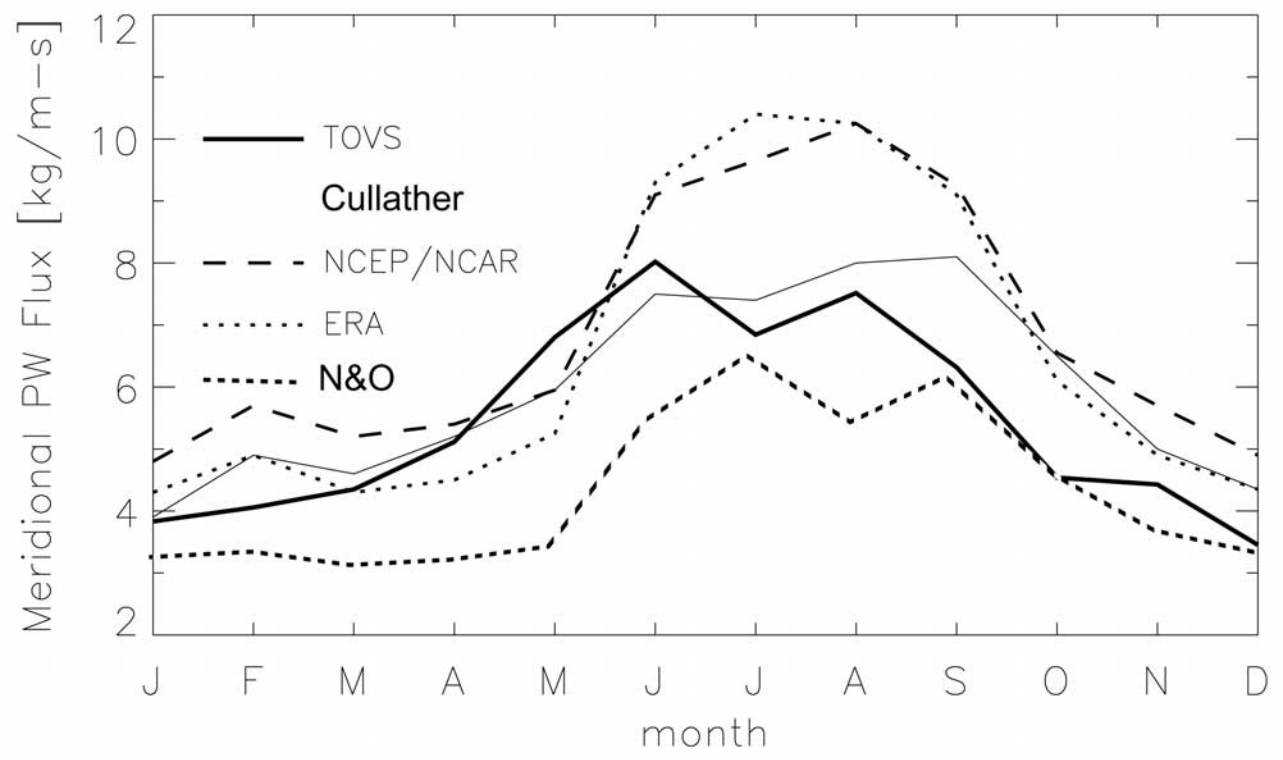

Figure 16. Annual cycle of meridional vapor transport across 70°N from TOVS (heavy solid), *Cullather et al.* [2000] rawinsonde (thin solid), *Nakamura and Oort* [1988] rawinsonde (heavy dotted), ERA (light dotted), and NCEP-NCAR reanalysis (dashed). Reanalysis data are from *Cullather et al.* [2000]. TOVS data are for 1980–1993, *Nakamura and Oort* [1988] are for 1963–1973, and all other data are for 1979–1993.

calculations will show erroneously high *PW* convergence over these regions. This may, in fact, explain the strong summer *PW* convergence seen in the NCEP-NCAR reanalysis but not in the rawinsonde or TOVS data. Apparent deficiencies in upper-level wind fields are also a possible source of bias in comparing rawinsonde convergences to those derived from reanalyses or TOVS, as the latter two calculations use the same wind fields. If the results of our wind validaton (Figure 6) are consistent across the region, we would expect that wind errors would contribute negative biases to TOVS and reanalysis poleward moisture transport. Despite the differences between the TOVS, rawinsonde, and reanalysis calculations during the summer, it is clear that the new TOVS estimate presents a realistic depiction of the annual cycle of *PW* flux across 70°N.

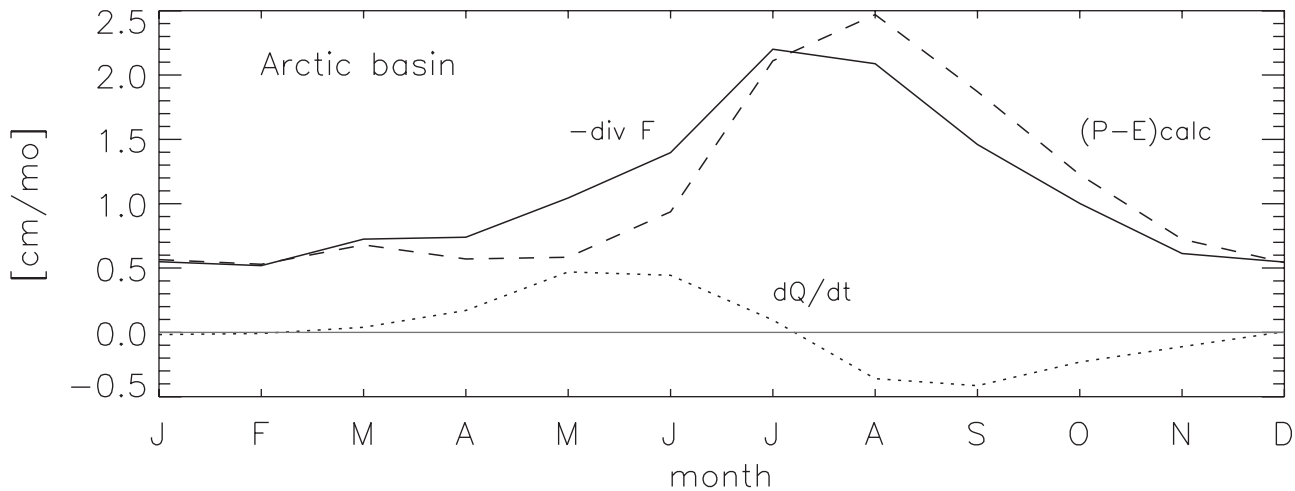

Figure 17. Climatological annual cycle of TOVS moisture budget components over the Arctic basin (regions 1–7): $\left(-\nabla \cdot \vec{F}\right)/\rho_w$ (solid), $(P\text{-}E)_{\text{calc}}$ (dashed), $\partial Q/\partial t$ (dotted) from 1980–1998.

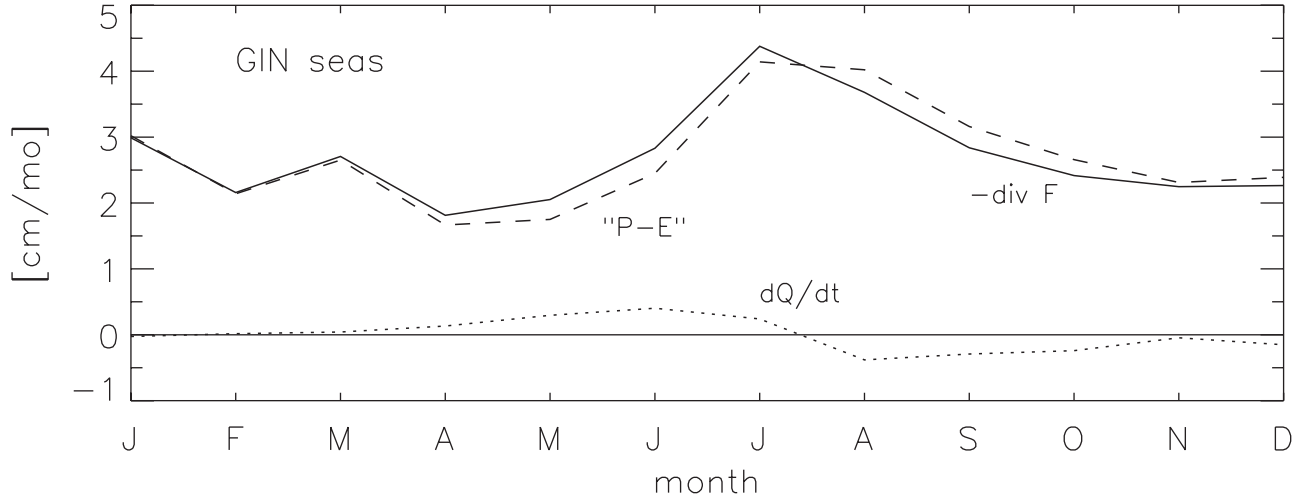

Figure 18. Climatological annual cycle of TOVS moisture budget components over the GIN seas (region 9): $\left(-\nabla \cdot \vec{F}\right)/\rho_w$ (solid), $(P\text{-}E)_{\text{calc}}$ (dashed), $\partial Q/\partial t$ (dotted) from 1980–1998.

[59] There are striking differences between the annual cycles of the moisture budget components (net precipitation, *PW* flux convergence, and *PW* tendency) over the Arctic basin (Figure 17) and the GIN Seas (Figure 18). Over the Arctic basin both net precipitation and flux convergence show a strong summer maximum of more than 2 cm mo^{-1} (four times the winter rate). The *PW* tendency curve shows that the summer *PW* peak is brief: *PW* begins decreasing right after it peaks in late July. In contrast, the winter *PW* levels are constant from mid-December to mid-March. During the transition months (when the monthly *PW* tendency is strongly positive or negative), changing *PW* accounts for a substantial portion of the total flux convergence. In May, for example, about 50% of the *PW* flux convergence results in increased moisture storage over the Arctic basin. Over the GIN Seas, in contrast, flux convergence exhibits a less defined annual cycle and varies only by a factor of two, peaking in July at 4 cm mo^{-1} with minima of about 2 cm mo^{-1} in the transition seasons. The *PW* tendency term is considerably less important, resulting in a near equivalence of $\left(-\nabla \cdot \vec{F}\right)/\rho_w$ and $(P\text{-}E)_{\text{calc}}$.

[60] Averaged over the Arctic basin, the high-frequency transient component of *PW* flux convergence makes the largest contribution to the total throughout the year (Figure 19). The inter-monthly mean contribution increases during the summer months corresponding to the summertime low pressure and associated convergence in the wind field. From November through February, transients contribute about 85% of the total over the Arctic basin. This contribution decreases to about 65% of the total in July. In contrast, over the GIN Seas the mean flow around the Icelandic low (present in most months) results in substantial inter-monthly mean contributions to the total *PW* convergence (not shown). In fact, for six months of the year (July December), the mean and transient convergence components are about equal. From January–March, the inter-monthly mean contribution predominates owing to wind convergence around the very strong Icelandic low. During

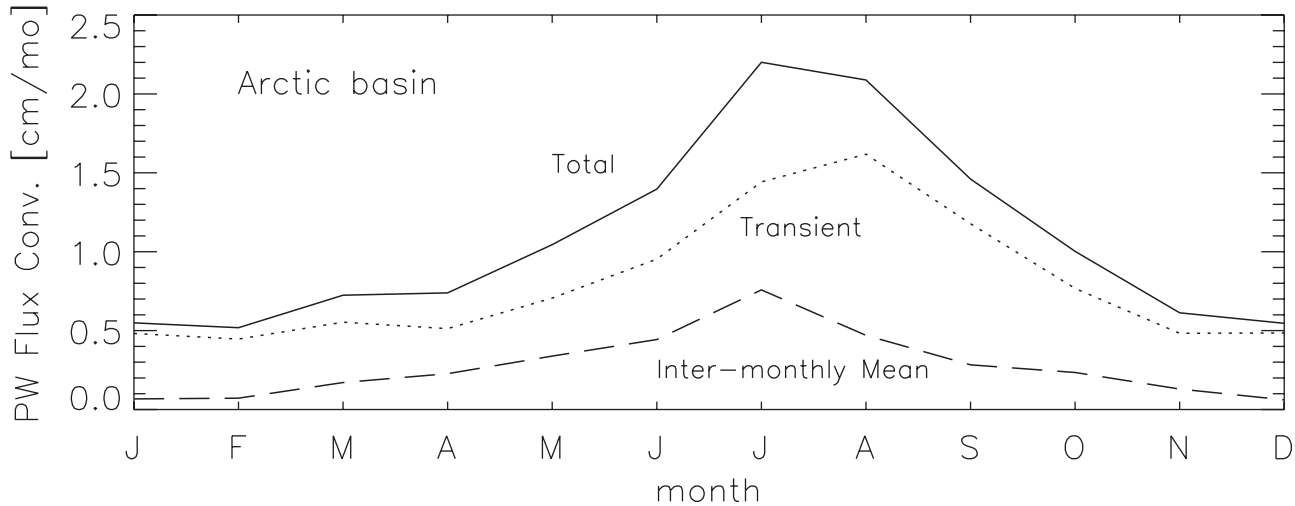

Figure 19. Climatological annual cycles of TOVS-computed total, inter-monthly mean, and high-frequency transient contributions to precipitable water flux convergence over the Arctic Basin (regions 1–7) in cm mo^{-1} from 1980–1998.

May and June, the inter-monthly mean contribution decreases because of the relatively weak Icelandic low.

6. Summary and Conclusions

[61] This paper describes the method used to generate a new, 19-year, satellite-derived data set of daily moisture budget quantities for the Arctic basin. We combine precipitable water retrievals from the NASA/NOAA TOVS Polar Pathfinder data set with upper-level winds from the NCEP-NCAR Reanalysis to obtain fields of corrected precipitable water (*PW*), *PW* flux, and net precipitation (*P-E*) at (100 km)^2 resolution across the region north of 60°N. In addition to the techniques used to create the data set, we also present validation results, annual and monthly climatologies, and relative contributions by transient and inter-monthly mean circulation features.

[62] Our initial validation efforts reveal that *PW* fields retrieved from TOVS satellite data appear to be lower than a rawinsonde-derived *PW* climatology by approximately 18% on average across the Arctic basin. Annual mean errors over sea ice are explained primarily (79%) by deficiencies in the TOVS retrieval algorithm to account for the effects of cloud, and over land areas 41% of the error is related to retrieval errors caused by high elevation. Moist biases in humidity sensors on rawinsondes have been reported for cold conditions, and this source of error may account for some of the difference we observe. Our empirical corrections–applied separately over land, ice, and open ocean–reduce the apparent error from 18% to 2%.

[63] Using corrected TOVS *PW* retrievals combined with NCEP-NCAR Reanalysis upper-level winds, we generate daily fields of *PW* flux and net precipitation from October 1979 through December 1998. Our values agree well with fields derived from reanalysis products in areas where rawinsondes are dense, thereby verifying the credibility of the satellite-derived quantities. In regions where assimilation data are sparse (e.g., most of the Arctic Ocean), however, TOVS values differ significantly from *PW* fluxes calculated from reanalysis data, suggesting that reanalysis products are less reliable in these areas. Our analysis implies that the reanalysis centers should review their methods to ingest moisture data from rawinsondes in the Arctic, perhaps allowing their radius of influence to increase, and also to consider incorporating moisture information either directly as radiances from moisture-sensitive satellite channels or from retrievals of geophysical quantities.

[64] This new data set captures the known climatological patterns of moisture fluxes, including the annual-mean cyclonic transport of moisture within the Arctic basin and annual cycles of the flux and net precipitation that peak in summer months. Differences between TOVS values and estimates from other sources (Table 2) originate from smaller poleward fluxes from TOVS in the eastern Arctic and larger equatorward fluxes in the west. This implies that moisture gradients in TOVS fields are larger than those from other sources. We believe that TOVS-derived moisture gradients are more accurate than values based on rawinsondes and reanalyses owing to the lack of conventional data for assimilation over most of the central Arctic Ocean.

[65] Examination of the contribution to *PW* flux and net precipitation by transient circulation features reveals the importance of transient processes to the moisture budget. Over the Arctic, 74% of net precipitation is due to transport by transient eddies; this contribution varies regionally from 32% in the GIN Seas to 90% in the Nansen Basin.

[66] In addition to the analyses reported here, the potential applications of this new moisture budget data set are considerable. Net precipitation is an important input for sea ice models, and model results can gain realism by assimilating time-varying fields of net precipitation. Increased temporal and spatial resolution of net precipitation will benefit estimates of the freshwater budget of the Arctic Ocean. Finally, careful analysis of trends in precipitable water, *PW* fluxes, and *P-E* will help elucidate relationships between changes in the global climate and the Arctic moisture budget. This issue is addressed by *Groves and Francis* [2002].

[67] **Acknowledgments.** This research was supported by an NSF Graduate Research Fellowship, NASA Grant NAGW 2407 (POLES) and NSF Grant SGER:0105461. The authors would like to thank Drew Rothrock for his extensive guidance and assistance, as well as Mike Wallace, David Battisti, and Axel Schweiger. We also thank the anonymous reviewers for their many constructive comments. We are grateful to Mark Ortomeyer for his computing support and encouragement.

References

Briazgin, N. N., L. P. Burova, and V. P. Khrol, *Atlas of the Water Balance of the Northern Polar Area* (in Russian), 82 pp., Gidrometeoizdat, St. Petersburg, Russia, 1996.

Broecker, W. S., Ocean circulation; An unstable superconveyor, *Nature*, *367*(6462), 414–415, 1994.

Bromwich, D. H., R. I. Cullather, and M. C. Serreze, Reanalysis depictions of the Arctic atmospheric moisture budget, in *The Freshwater Budget of the Arctic Ocean*, edited by E. L. Lewis, pp. 163–196, Kluwer Acad., Norwell, Mass., 2000.

Cavalieri, D. J., P. Gloersen, C. L. Parkinson, J. C. Comiso, and H. J. Zwally, Observed hemispheric asymmetry in global sea ice changes, *Science*, *278*(5340), 1104–1106, 1997.

Chédin, A., N. A. Scott, C. Wahiche, and P. Moulinier, The Improved Initialization Inversion method: A high resolution physical method for temperature retrievals from the TIROS-N series, *J. Clim.*, *24*, 124–143, 1985.

Cullather, R. I., D. H. Bromwich, and M. C. Serreze, The atmospheric hydrologic cycle over the Arctic Basin from reanalysis, part I, Comparison with observations and previous studies, *J. Clim.*, *13*, 923–937, 2000.

Elliot, W. P., and D. J. Gaffen, On the utility of rawinsonde humidity archived for climate studies, *Bull. Am. Meteorol. Soc.*, *72*, 1507–1520, 1991.

Francis, J. A., Improvements to TOVS retrievals over sea ice and applications to estimating Arctic energy fluxes, *J. Geophys. Res.*, *99*(D5), 10,395–10,408, 1994.

Francis, J. A., Validation of reanalysis upper-level winds in the Arctic with independent rawinsonde data, *Geophys. Res. Lett.*, *29*(9), 1315, doi:10.1029/2001GL014578, 2002.

Francis, J. A., and A. J. Schweiger, A new window opens on the Arctic, *Eos Trans. AGU*, *81*(8), 77,83, 2000.

Gaffen, D. J., and W. P. Elliott, Column water vapor content in clear and cloudy skies, *J. Clim.*, *6*, 2278–2287, 1993.

Gloersen, P., W. J. Campbell, D. J. Cavalieri, J. C. Comiso, C. L. Parkinson, and H. J. Zwally, Arctic and Antarctic sea ice, 1978–1987: Satellite passive microwave observations and analysis, *NASA Spec. Publ. 511*, 290 pp., 1992.

Groves, D. G., The moisture budget of the Arctic atmosphere from TOVS satellite data, M.S. thesis, Univ. of Wash., Seattle, Wash., 2001.

Groves, D. G., and J. A. Francis, Variability of the Arctic atmospheric moisture budget from TOVS satellite data, *J. Geophys. Res.*, *107*, doi:10.1029/2002JD002285, in press, 2002.

Johannessen, O. M., E. V. Shalina, and M. W. Miles, Satellite evidence for an Arctic sea ice cover in transformation, *Science*, *286*, 1937–1939, 1999.

Kahl, J. D. W., N. A. Zaitseva, V. Khattatov, R. C. Schnell, D. M. Bacon, J. Bacon, V. Radionov, and M. C. Serreze, Radiosonde observations from the former-Soviet "North Pole" series of drifting ice stations, *Bull. Am. Meteorol. Soc.*, *80*, 2019–2026, 1999.

Kalnay, E., et al., The NCEP/NCAR 40-year reanalysis project, *Bull. Am. Meteorol. Soc.*, *77*(3), 437–471, 1996.

Key, J. R., and A. C. K. Chan, Multidecadal global and regional trends in 1000 mb and 500 mb cyclone frequencies, *Geophys. Res. Lett.*, *26*(14), 2053–2056, 1999.

Legates, D. R., and C. J. Willmott, Mean seasonal and spatial variability in gauge-corrected global precipitation, *Int. J. Climatol.*, *10*, 111–133, 1990.

Martin, S., and E. A. Munoz, Properties of the Arctic 2-meter air temperature field for 1979 to the present derived from a new gridded data set, *J. Clim.*, *10*(6), 1428–1440, 1997.

Maslanik, J. A., M. C. Serreze, and R. G. Barry, Recent decreases in Arctic summer ice cover and linkages to atmospheric circulation anomalies, *Geophys. Res. Lett.*, *23*(13), 1677–1680, 1996.

Maslanik, J. A., M. C. Serreze, and T. Agnew, On the record reduction in 1998 western Arctic sea-ice cover, *Geophys. Res. Lett.*, *26*, 1905–1908, 1999.

Masuda, K., Atmospheric heat and water budgets of the polar regions: Analysis of FGGE data, *Proc. NIPR Symp. Polar Meteorol. Glaciol.*, *3*, 79–88, 1990.

Morison, J., M. Steele, and R. Andersen, Hydrography of the upper Arctic Ocean measured from the nuclear submarine U.S.S. Pargo, *Deep Sea Res.*, *Part I*, *45*(1), 15–38, 1998.

Nakamura, N., and A. H. Oort, Atmospheric heat budgets of the polar regions, *J. Geophys. Res.*, *93*, 9510–9524, 1988.

National Snow and Ice Data Center (NSIDC), Daily Arctic ocean rawinsonde data from Soviet drifting ice stations, *NSIDC-0060* (CD-ROM), Univ. of Colo., Boulder, Colo., 1997a.

National Snow and Ice Data Center (NSIDC), NCEP/NCAR Arctic Marine Rawinsonde Archive, *NSIDC-0054*, Univ. of Colo., Boulder, Colo., 1997b.

Pexioto, J. P., and A. H. Oort, *Physics of Climate*, 520 pp., Am. Inst. of Phys., New York, 1992.

Radionov, V. F., N. N. Bryazgin, and E. I. Alexandrov, The snow cover of the Arctic basin, *TR 9701*, 95 pp., Appl. Phys. Lab., Univ. Wash., Seattle, Wash., 1997.

Rigor, I. G., R. L. Colony, and S. Martin, Variations in surface air temperature observations in the Arctic, 1979–1997, *J. Clim.*, *13*, 896–914, 2000.

Rothrock, D. A., Y. Yu, and G. A. Maykut, Thinning of the Arctic sea-ice cover, *Geophys. Res. Lett.*, *26*(23), 3469–3472, 1999.

Schweiger, A. J., R. W. Lindsay, J. R. Key, and J. A. Francis, Arctic clouds in multiyear satellite data sets, *Geophys. Res. Lett.*, *26*(13), 1845–1848, 1999.

Schweiger, A., R. W. Lindsay, J. A. Francis, J. R. Key, J. Intreiri, and M. Shupe, Validation of TOVS Path-P data during SHEBA, *J. Geophys.*, *107*, doi:10.1029/2000JC000453, in press, 2002.

Scott, N. A., A. Chedin, R. Armante, J. Francis, C. Stubenrauch, J.-P. Chaboureau, F. Chevallier, C. Claud, and F. Cheruy, Characteristics of the TOVS Pathfinder Path-B data set, *Bull. Am. Meteorol. Soc.*, *80*, 2679–2701, 1999.

Serreze, M. C., and R. G. Barry, Atmospheric components of the Arctic Ocean hydrologic budget assessed from rawinsonde data, in *The Freshwater Budget of the Arctic Ocean*, edited by E. L. Lewis, pp. 141–161, Kluwer Acad., Norwell, Mass., 2000.

Serreze, M. C., and C. M. Hurst, Representation of mean Arctic precipitation from NCEP-NCAR and ERA Reanalyses, *J. Clim.*, *13*, 182–201, 2000.

Serreze, M. C., J. A. Maslanik, M. C. Rehder, R. C. Schnell, J. D. Kahl, and E. L. Andreas, Theoretical heights of buoyant convection above open leads in the winter Arctic pack ice cover, *J. Geophys. Res.*, *97*, 9411–9422, 1992.

Serreze, M. C., M. C. Rehder, R. G. Barry, and J. D. Kahl, A climatological database of Arctic water vapor characteristics, *Polar Geogr. Geol.*, *18*(1), 63–75, 1994.

Serreze, M. C., R. G. Barry, and J. E. Walsh, Atmospheric water vapor characteristics at 70 deg N, *J. Clim.*, *8*, 719–731, 1995a.

Serreze, M. C., M. C. Rehder, R. G. Barry, J. D. Kahl, and N. A. Zaitseva, The distribution and transport of atmospheric water vapor over the Arctic basin, *Int. J. Climatol.*, *15*(7), 709–727, 1995b.

Serreze, M. C., F. Carsey, R. G. Barry, and J. C. Rogers, Icelandic low cyclone activity: Climatological features, linkages with the NAO, and relationships with recent changes in the Northern Hemisphere circulation, *J. Clim.*, *10*(3), 453–464, 1997.

Serreze, M. D., J. E. Walsh, F. S. Chapin III, T. Osterkamp, D. Dyurgerov, V. Romanovsky, W. C. Oechel, J. Morison, T. Zhang, and R. G. Barry, Observational evidence of recent change in the northern high-latitude environment, *Clim. Change*, *46*, 159–207, 2000.

Steele, M., and T. Boyd, Retreat of the cold halocline layer in the Arctic Ocean, *J. Geophys. Res.*, *103*(C5), 10,419–10,435, 1998.

Steele, M., D. Thomas, D. A. Rothrock, and S. Martin, A simple model study of the Arctic Ocean freshwater balance, 1979–1985, *J. Geophys. Res.*, *101*(C9), 20,833–20,848, 1996.

Thompson, D. W. J., and J. M. Wallace, The Arctic Oscillation signature in the wintertime geopotential height and temperature fields, *Geophys. Res. Lett.*, *25*(9), 1297–1300, 1998.

Walsh, J. E., W. L. Chapman, and T. L. Shy, Recent decrease of sea level pressure in the central Arctic, *J. Clim.*, *9*(2), 480–486, 1996.

Walsh, J. E., X. Zhou, D. Portis, and M. C. Serreze, Atmospheric contribution to hydrologic variations in the Arctic, *Atmos. Ocean*, *32*(4), 733–755, 1994.

J. A. Francis, J. J. Howard Marine Laboratory, Institute of Marine and Coastal Sciences, Rutgers University, 74 Magruder Road., Highlands, NJ 07732, USA. (francis@imcs.rutgers.edu)

D. G. Groves, RAND Graduate School, P. O. Box 2138, Santa Monica, CA 90407-2138, USA. (groves@rgs.edu)